Miguel Mota Prego Rosmaninho

Electrodeposition of Bi_2Te_3 Nanomaterials for Thermoelectric generators

Department of Physics and Astronomy
Faculty of Sciences of the University of Porto
September 2014

Electrodeposition of Bi_2Te_3 Nanomaterials for Thermoelectric generators

Thesis submitted to the
Faculty of Sciences of the University of Porto
in partial fulfilment of the requirements
for the degree of
Master in Physics Engineering

Supervisor: Dr. André Miguel Trindade Pereira
co-Supervisor: Dra. Mariana de Jesus Paiva Proença

Department of Physics and Astronomy
Faculty of Sciences of the University of Porto
September 2014

“When you reach for the stars, you may not quite get them,

but you won’t come up with a handful of mud either.”

Leo Burnett

Acknowledgements

First and foremost I want to thank my supervisor, André Miguel Trindade Pereira for his dedication, patience and support. I am very thankful for his continuous resourcefulness and for providing me the opportunity to develop this work. This would not be possible without him. I've learnt a great deal of things and it is all thanks to his efforts.

I also want to thank my co-supervisor, Dra. Mariana de Jesus Paiva Proença for all she taught me, for all the patience to deal with me and to expertly explain so many techniques and experimental details.

Special attention and thanks to all the inanoE members for the interest shown in this work and the investment made in me.

Special thanks to my family, more specifically my parents and my brother for making me who I am today and for giving me all the love and caring that very few people have the chance to experience. You have given me what I can never repay you.

I want to also thank Ana Pires, thanks to you several of my more boring days were a lot funnier and without your help, I'd have burnt many more things in those ovens. You've been quite important for this work and, even though we still do not understand why, I want to thank you for trying to enter this area by depositing Bi_2Te_3 in the electron beam deposition, even if it wasn't your plan.

I would like to also show my gratitude to Bernardo Bordalo and Filipe Falcão for all the laughing, support and interest you have shown in our friendship. This would definitely be much harder experience without the relaxation periods you have given me and all the patience you have shown. Thank you, really. I would like to also thank Óscar Moutinho, Ana Rodrigues, Ana Fernandes and Eliana for the friendship we share and the support you gave me. Thanks for all the good times.

I would also like to thank all the members of IFIMUP-IN, like Célia Sousa and João Ventura but I would like to give a special focus to Francisco Carpinteiro for the great work and time he dispensed to help me in this. A part of this work would have not been possible without him and it was quite an important personal achievement what he helped me optimize.

It is quite important to refer all the hard work and kindness shown to me by "UNIDADE DE MICROSCOPIA ELETRÓNICA" of Vila-Real specifically Lisete Fernandes and Pedro Tavares. I would also like to thank Sofia Teixeira, the PEEC student who diligently did the COMSOL simulations and has shown so much interest in this area.

Finally, the most important person I have in my life and which I need to thank the most, Ana Cláudia Teixeira thank you for all your dedication, love and patience for me. You have given me more support than I could have thought possible and this work is, in part, your doing and yours as well. Thank you, really.

Resumo

O consumo energético atual é o mais alto de sempre, aumentando por isso a procura por novos e inovadores geradores baseados em métodos verdes. É imperativo que estes dispositivos sejam sustentáveis e usem fontes não convencionais para conquistarem o seu espaço. É aqui que a tecnologia termoelétrica é única, conquistando o grande mercado que é o de energia calorífica desperdiçada. O princípio por detrás destes materiais é utilizar um gradiente de temperatura para gerar uma corrente elétrica, utilizando o efeito de Seebeck e Peltier.

Este trabalho inicia-se com uma breve explicação das técnicas utilizadas assim como das desenvolvidas unicamente para a medição de propriedades termoelétricas. Uma explicação completa do método de eletrodeposição é dada, seguida do método de produção da alumina anódica nanoporosa. O trabalho continua com a elaboração sobre os filmes finos de Bi_2Te_3 electrodepositados no regime potentioestático. Aqui mostrou-se a habilidade de criar ambos o tipo p e n de Bi_2Te_3 nomeadamente estudando a estequiometria, cristalografia, morfologia e processos de crescimentos das amostras. Uma relação foi estabelecida entre o potential de eletrodeposição aplicado e estas propriedades, assim como o efeito nas amostras de variar a concentração dos iões de Bi e Te no eletrólito.

Utilizando o conhecimento obtido na preparação destes filmes finos, o crescimento de nanofios de Bi_2Te_3 assistida pela alumina anódica nanoporosa será mostrada. Uma forte relação entre o potencial de eletrodeposição e a taxa de deposição, preenchimento dos poros, estequiometria e cristalografia dos nanofios é apresentada, tendo sido concluído que potenciais baixos mostram um crescimento cristalino quase único. Além disso, completo preenchimento dos poros com a estequiometria quase perfeita de 2:3 de Bi/Te será demonstrada, que rapidamente se torna amorfa, com menor raio dos nanofios e uma estequiometria muito distinta com o crescimento deste potencial.

Os últimos resultados encontram-se baseados na aplicação dos resultados anteriores na criação de um protótipo de um microgerador. Só um dos *designs* desenvolvidos foi produzido, utlizando técnica litográficas para criar um conjunto de 100 pilares com 500 μm de diâmetro, criando assim um dispositivo com uma área de 1 cm^2. Baseado na criação de pilares de Bi_2Te_3 criados via eletrodeposição, foi possível provar que dispositivos tanto de tipo p como de tipo n foram desenvolvidos e que estes são capazes de produzir um potencial constante acima dos 10 μV. Simulações numéricas foram também realizadas com estruturas similares o que mostrou que o dispositivo desenvolvido apresenta valores abaixo do teórico. Uma metodologia foi também proposta para construir e desenvolver um dispositivo completamente funcional que contenha pilares de ambos os tipos, p e n, que irá mostrar uma potência muito superior e que será um microgerador completamente aplicável.

Abstract

Present energy consumption is the highest that has ever been, boosting the need for new, innovative generators based on green methods. It is imperative that these devices are self-sustained and use non-conventional sources to conquer their space. This is where the thermoelectric technology can be unique, by conquering the big market that is wasted heat energy. The physical principle behind these materials is utilizing a gradient of temperature to generate an electrical current, the so called Seebeck and Peltier effect.

This work starts with a brief overview of the techniques used as well as the ones developed solely for the measurement of thermoelectric properties. A thorough explanation of the electrodeposition process is given, followed by the production of porous anodic alumina templates. The work proceeds with the elaboration of thin films structures of Bi_2Te_3 electrodeposited in a potenstiotatic regime. Here was shown the ability to create both p and n type Bi_2Te_3 namely by studying the stoichiometry, crystallography, morphology and general growth processes of the samples. A relation was established between the electrodeposition potential applied and these properties, as well as the effects of varying the concentration of Bi and Te ions in the electrolyte on the samples.

By using the knowledge obtained in the thin films preparations, the growth of Bi_2Te_3 nanowires assisted by the porous anodic alumina template will be shown. A strong relation between the electrodeposition potential and the deposition rate, pore filling, stoichiometry and crystallography of the nanowires is presented, having been concluded that low deposition potentials show almost single crystalline growth. Furthermore, complete pore filling with a 2:3 Bi/Te ratio will be shown, which quickly turns amorphous, with smaller nanowire radius and very distinct stoichiometry with the growth of this potential.

The final results are based on the application of all the previous work (chapter 3 and 4) in the creation of working microgenerator prototypes. Only one of the designs was produced using lithographic techniques to create an array of 100 pillars with 500 μm in diameter making a device with an area of 1 cm^2. Based on the creation of Bi_2Te_3 pillars made via electrodeposition, it was possible to prove that both n and p type devices were produced and that these are capable of producing a continuous potential of over 10 μV. Numerical simulations were also performed with similar structures which showed that our developed device presents much lower values. It has also been proposed one methodology to build and develop a fully functional device encompassed of both p and n type pillars which should prove to have much higher power output and to be an applicable microgenerator.

Contents

List of Figures

List of Tables

Nomenclature

Bi_2Te_3	Bismuth telluride
EDS	Energy-dispersive X-ray spectroscopy
ITO	Indium tin oxide
PAA	Porous anodic alumina
PMMA	Poly(methyl methacrylate)
SEM	Scanning electron microscope
XRD	X-ray diffraction
zT	Figure of merit

Chapter 1
Introduction

1.1 Thermoelectric effect

The permanent requirement for energy in the world and the rise on environmental awareness boost the demand for new clean sources. The most prominent energy sources are based on combustion or heating processes [Figure 1.1 (a)], with 60% of their energy wasted in the form of heat [1]. This opens the pathway for heat recovering by converting it into electrical energy for power supply devices. Thermoelectric technology arises as the best solution for this issue since it has the ability to create current from a temperature gradient (and vice-versa). Furthermore, it has no moveable parts, it is emission free, silent and a vibration free principle. It also presents very low maintenance costs, the ability to control the amount of wasted heat leaked into the environment and a very user friendly working process, which are vital advantages for the market. In fact, this technology already represents a market of 175-200 million Euros, as reported in *ObservatoryNano june 2011* [1] [Figure 1.1 (b)] and, even though it is a market of millions, thermoelectric devices are seen as being in the prototype phase.

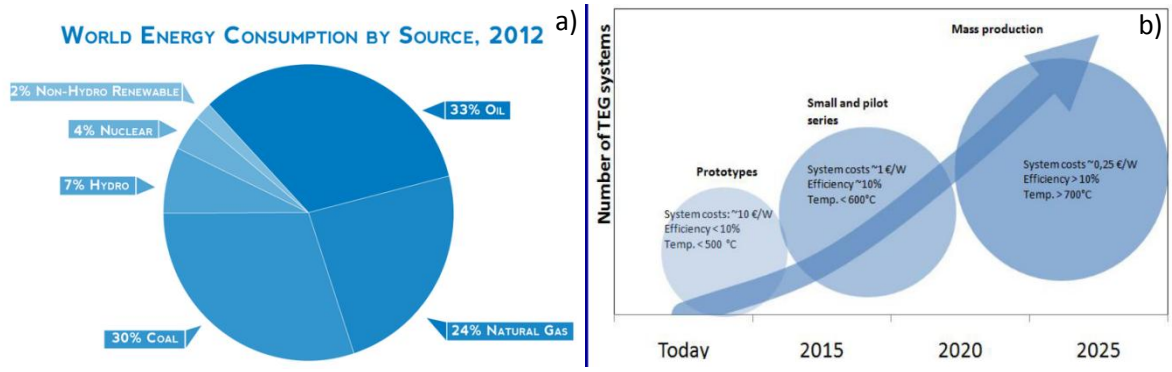

Figure 1.1 (a) World energy consumption reported in the *bp statistical review of World Energy* [2]. (b) Thermoelectric devices growth projections reported in *ObservatoryNano june 2011* [1].

Several predictions state that it will easily grow 10-100 times due to the optimization and new low cost manufacturing processes being reported in the most recent scientific works [3-6]. One of the most important characteristics is that it works in parallel to other energy sources instead of competing with them. As an example, on the transportation sector alone, these devices could quickly, and very conservatively, represent a 7 billion euro market [1], without even counting the market for thermal control that thermoelectric air conditioners or seat heater/cooler systems could bring. Several companies have already started investing and proving the power behind this concept, such as Vodafone's Power Pocket, BMW's award winning thermoelectric generator [7] or Fujifilm's high performance organic thermoelectric [8] [Figure 1.2]. All of these applications are but a fraction of its potential uses, since it has predicted uses in medicine, where our body heat versus air temperature

could be used to fuel small devices such as pacemakers, in biomass facilities, where the heat released during fermentation could be harvested and many others situations [4].

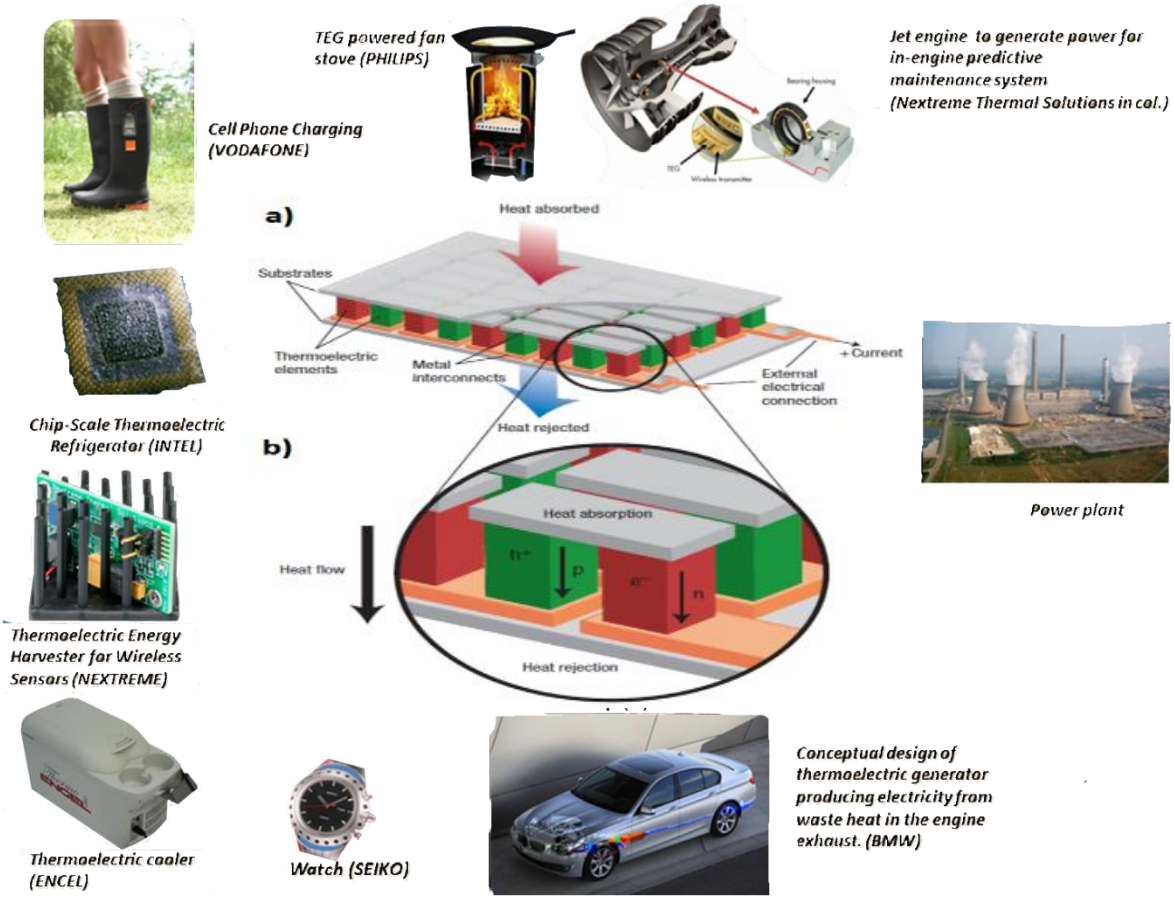

Figure 1.2 Several examples for the use of thermoelectrics in today's market, adapted from [4].

There are already a few configurations for thermoelectric devices, but the most common are based on the working principle represented in Figure 1.2. The basic unit of a thermoelectric cell is composed of an n-type and a p-type semiconductor (two legs), connected to each other via a conducting material. The use of a combination of p and n-type is due to the opposite signal of the respective Seebeck coefficient which is a condition to ensure the current flow through both legs. The main thermoelectric materials used are thus semiconductors and insulators [Figure 1.3 (a)], due to the high Seebeck coefficient they present, when compared to the very low values of metals and other conductive materials. In fact, the Seebeck phenomenon was discovered in 1821 by Thomas Seebeck and gave the relation between the electrical potential and temperature gradient [9]:

$$\mathbf{\Delta V = S \Delta T} \tag{1.1}$$

where S is the Seebeck coefficient, which is negative for n-type semiconductors and positive for p-type semiconductors. Microscopically, when an n-type or p-type material is under a temperature gradient (ΔT) between the two extremities, the carriers on the hot side (T_h) of the bar will have a higher energy, which is reflected in a longer mean free path [Figure 1.3 (b)]. As such, the probability

of these carriers to diffuse to the other side is much larger than the opposite happening, creating a concentration of charge on the cold side (T_c) which leads to an electrical field (E) [Figure 1.3 (c)] [11]. This creates a current from the hot extremity to the cold extremity in the case of holes and the inverse in the case of electrons. The Peltier effect uses the inverse principle, where an electrical field will dislocate these carriers from one side to the other. These high energy carriers will then heat up one side of the bar while the other side cools down, creating a temperature gradient.

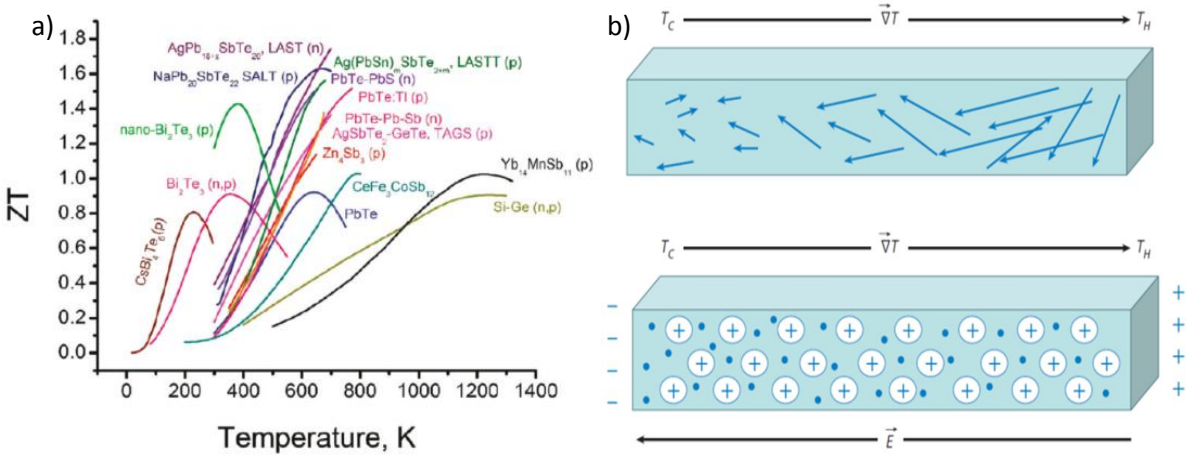

Figure 1.3 Best thermoelectric for each temperature range [10]. Schematic representation of the thermoelectric effect showing carriers (b) mean free path length and (c) concentration along the bar [11].

These points are the main reason to use p and n type [Figure 1.2] to ensure that the current passes through.

1.2 Thermoelectric efficiency

It is well known that for a thermoelectric generator, the maximum efficiency of a device will be [12]:

$$\eta_{TE} = \frac{T_h - T_c}{T_h} \frac{\sqrt{1+zT}-1}{\sqrt{1+zT}+\frac{T_c}{T_h}} \tag{1.2}$$

where T_h and T_c are the hot and cold side temperatures, respectively, and zT is the figure of merit. The zT depends of the thermal transport properties of the material and is expressed as [13]:

$$zT = \frac{\sigma S^2}{K} T \tag{1.3}$$

where σ is the electrical conductivity, K is the thermal conductivity and T is the temperature.

This figure of merit was a major limitation for thermoelectrics since, as seen in Figure 1.4, until the early 2000's its maximum value was limited to 1. As is visible in Figure 1.5 (a) these low zT values do not allow high efficient thermoelectric devices to be developed.

Nowadays this limitation has been broken due to the implementation of several nanomaterials which had a tremendous increase of zT, to values of over 2.4 [5].

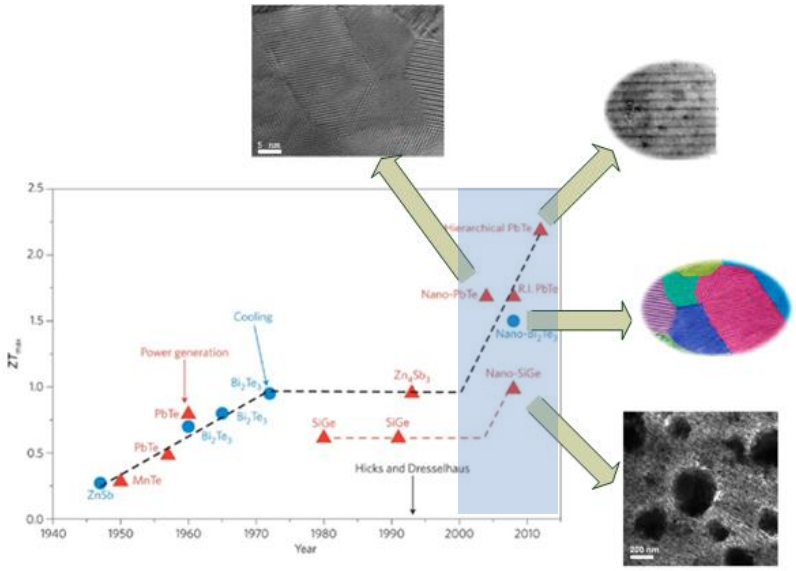

Figure 1.4 Most recent and successful developments in thermoelectric materials [14].

That improvement came mainly by increasing the phonon scattering within the unit cell through the creation of rattling structures or point defects such as interstitials, vacancies or by alloying. This has enhanced interfacial scattering using multiphase (disordered) nanocomposites or nanoscopic confined structures with a strong impact namely decreasing the thermal conductivity, raising the zT value and will be discussed in detail in the next section.

The impact of increasing the zT value is crucial for current scientific research, as indicated in Figure 1.5 (a), where in ideal conditions the thermoelectric generator efficiency could reach values as high as 45%. This, combined with their ability to be used in parallel to traditional power sources [Figure 1.5(b)] with efficiencies almost as high as them, could highly improve energy yields.

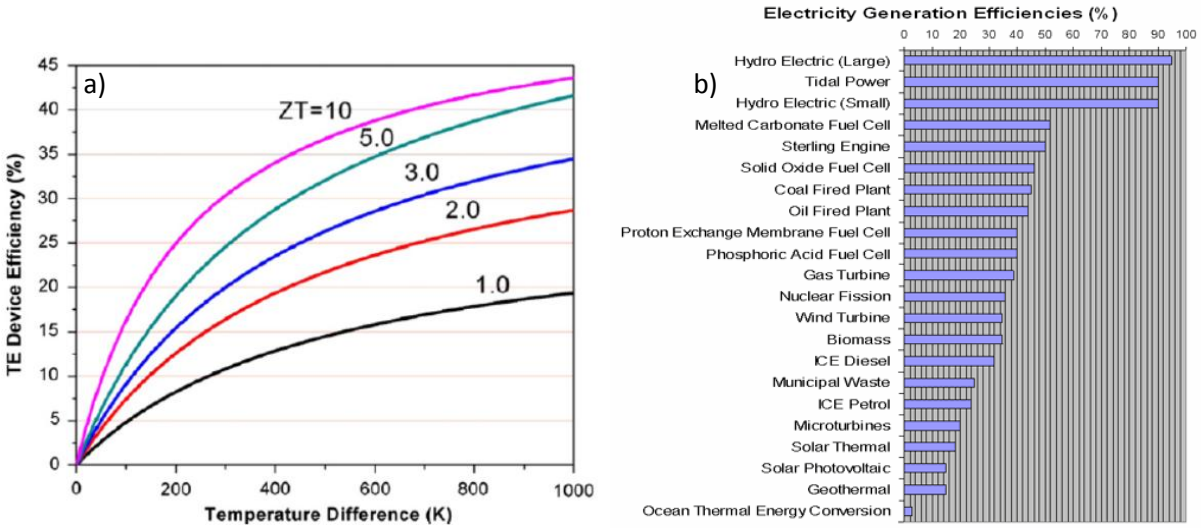

Figure 1.5 (a) Thermoelectric device efficiency with T_c= 300 K [15]. (b) Generation efficiencies of the most common energy sources [16].

1.3 Thermoelectric Bulk materials

The main strategies to increase the phonon scattering within the unit cell are being done in bulk materials, namely in skutterudites, clathrates, oxides and nanoinclusions.

1.3.1 Skutterudites and Clathrate

Skutterudites and clathrates possess interstitial voids in their unit cell, which can be filled with doping elements, in a cage-like structure [Figure 1.6 (a) and (b)]. The introduction of doping elements in the unit cell will lead to big atomic displacement which will translate in a rattling movement of the dopant in their site [17]. This vibration's frequency will vary with the atom, thus allowing one to tune the phonon scattering or to develop a multi-doped skutterudite which will scatter a wide range of phonons. Skutterudites are used mainly for high temperature ranges, having reached values of 1.7 zT at 850 K [18]. Still they have strong liabilities such as: long production times and the use of toxic elements like arsenium. The production times have been decreasing rapidly but the use of toxic elements is still an issue. On the other hand, clathrates use metal elements as doping agents but also use toxic elements. They are a recent technology, with many venues for potential improvements that might bring about further utilities. Still, zT's of 1.2 at 500 K have already been attained [19].

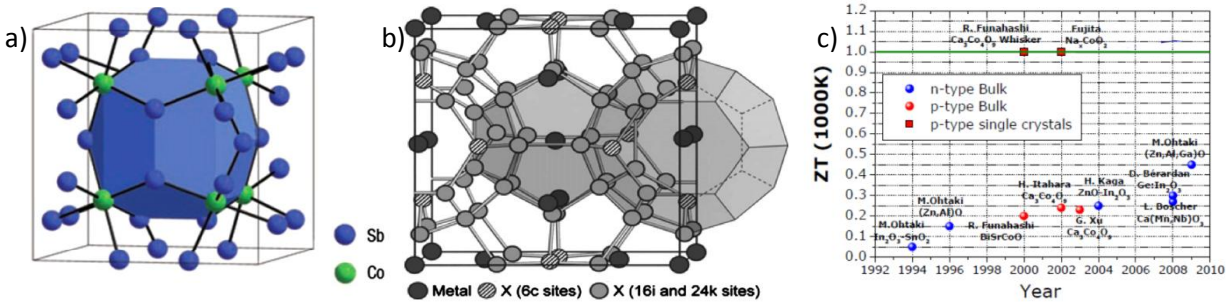

Figure 1.6 Crystal structures of (a) the skutterudite $CoSb_3$ and (b) a type-I clathrate [19]. The zT evolution for oxides over the last years (c) [20].

1.3.2 Oxides

Oxides are very important for high temperature, 1000 K or higher, thermoelectric materials. This kind of structure presents a zT of 1, and they are made of very common, low cost elements with no toxicity. Further development of these materials will allow the thermoelectric devices to recover heat on systems that have a high need for thermal-to-energy conversion, therefore they are the focus for big thermal power plants and big industrial high temperature devices. The interest in these materials was greatly spurred by Terasaki *et al.* [20] when they showed the great promise of $NaCo_2O_4$. Since then, several new works have been appearing having further roused the interest in thermoelectrics.

1.3.3 Composites: Nanoinclusions

Inclusions are small precipitations where the composition changes slightly when compared with the matrix around it, as can be seen in Figure 1.7 (a). These can be obtained by simple industrial

processes such as annealing and ball milling. They are seen as small scattering centres that dramatically increase the zT of known structures and materials. These inclusions take advantage of one of the main reasons for the increase in zT with the appearance of nano-engineering, which is the dramatic increase in the number of scattering centres for phonons without affecting the number of scattering centres for electrons. This is mainly due to the different length in the free mean path of these two types of particles. These very low cost improvements have already raised the maximum zT value of Bi_2Te_3 compounds by 50% to 1.56 zT [21].

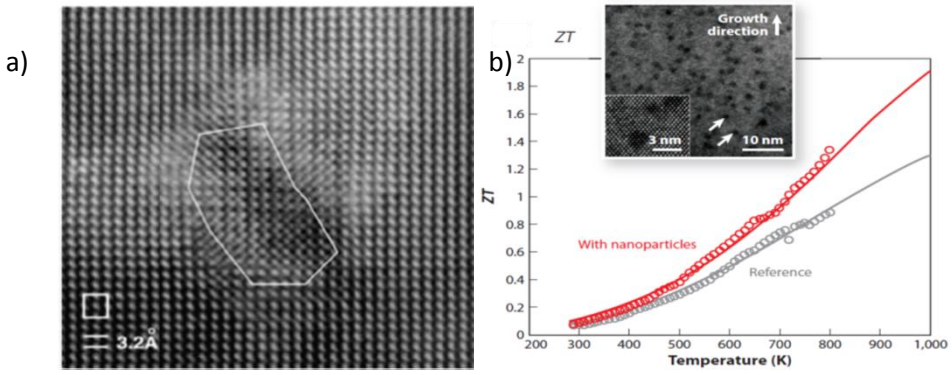

Figure 1.7 (a) Nano-inclusion of Ag-Sb in a $AgPb_{18}SbTe_{20}$ matrix [23]. (b) zT of 0.6% ErAs nanoparticles inside an $In_{0.53}Ga_{0.27}Al_{0.20}As$ matrix [22].

Another kind of nanoinclusions is the embedding of semi metallic nanoparticles into semiconductor matrices. This process is also very inexpensive, similar to the industrial processes referred above, as can be seen in Figure 1.7 (b), also having the advantage of being highly stable at high temperatures. This methodology of nanoinclusions is still in an early stage being foreseen as a good methodology to improve the zT.

1.4 Bismuth Telluride (Bi_2Te_3)

Bi_2Te_3 is the material with the highest zT value near room temperature, which makes it the most commonly used material in the thermoelectric market [Figure 1.3]. Since their discovery as excellent materials for thermoelectric technology, Bi_2Te_3 based materials reached improvements in zT higher than 50%, to over 1.5 zT [24]. This high efficiency is because Bi_2Te_3 is highly directional, which can be explained by its typical crystal structure, as depicted in Figure 1.8. In the c direction the bounds are of Van der Waals nature while covalent and ionic on the basal plane, which translates into a three times higher electrical conductivity for this plane. Furthermore, it possesses a high Seebeck coefficient since it is a semiconductor (around -200 μVK^{-1}), and a low thermal conductivity (around 1.20 $WK^{-1}m^{-1}$). In addition, the fact that it is compatible with almost every production method brings another great advantage to this material. Typical Bi_2Te_3 is used as an n-type semiconductor, but it can also be used as a p-type just by slightly changing the Bi:Te ratio. Experimentally it was observed that when there is a slight lack of Te in the composition (lower than 58%), it already presents a p-type behaviour.

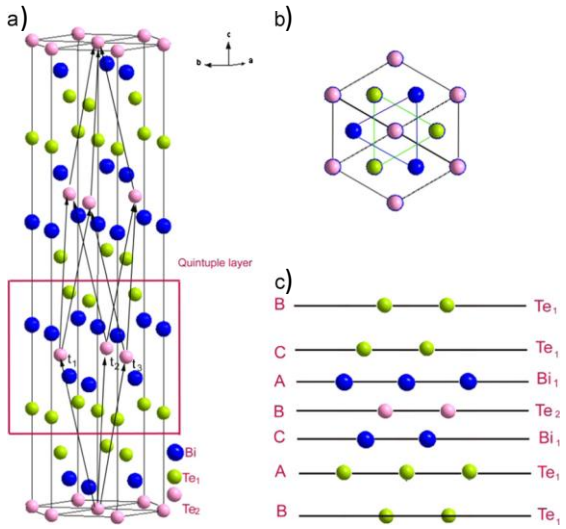

Figure 1.8 Crystal structure of Bi_2Te_3 [25].

1.5 Nanostructuring

As can be seen in Figure 1.9 and Figure 1.10, very low dimensional thermoelectrics could prove to have incredibly high zT values. This is a new line of thermoelectric research which grew in the mid 1990's and still continues on, aiming to reach record high zT values in the near future. These results were mainly obtained in two-dimensional or one-dimensional systems, which were composed of three main structures: (i) superlattices and quantum wells, (ii) nanowires and (iii) nanotubes.

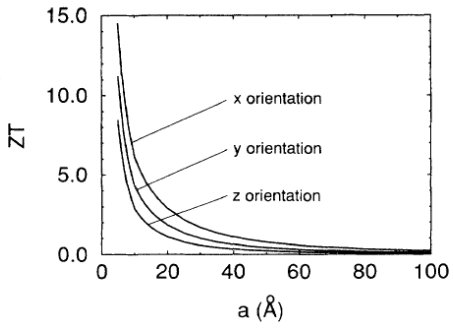

Figure 1.9 Plot of zT as a function of nanowire width along the x, y and z directions on Bi_2Te_3 [26].

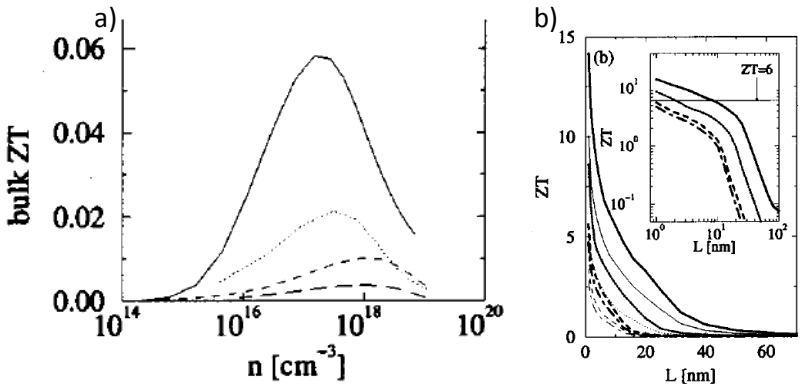

Figure 1.10 (a) Bulk zT value vs doping and (b) zT vs nanowire thickness [27].

1.5.1 Supperlattices and quantum wells

A superlattice is a series of alternated dominions, ranging from small composition changes to possible distinct compositions, having thicknesses from a few angstrom (Å) to several nanometers [Figure 1.11]. This approach produces better zT results than their bulk counterparts due to two main reasons: (i) the density of states near the Fermi level gets enhanced by the quantum confinement; and (ii) the phonons, in a wide range of frequencies, are strongly scattered on the interfaces between the different materials. Superlattices and quantum wells were the first indicators that interfaces were the fastest and easiest way to reach high zT, which spurred the growth of the bulk counterparts. Several works based on this phenomenon have already produced zT's over 2 [5].

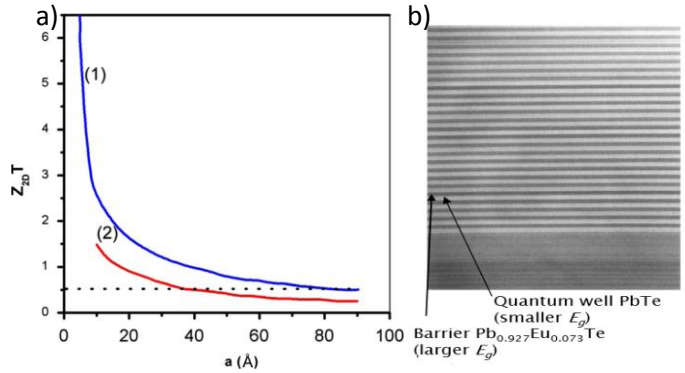

Figure 1.11 (a) Plot of zT vs layer thickness for the (1) a-b plane, (2) a-c plane of Bi_2Te_3 and the dashed line represents the bulk's zT [28]. (b) Example of a superlattice [29].

1.5.2 Nanowires and nanotubes

Having the highest predicted zT values, as seen in Figure 1.9, these are incredibly important structures for thermoelectrics. Nanowires are already being used in medicine, to dispense more localized treatments and with lesser doses; engineering, to improve solar panels; and environmental applications, such as water purification. In thermoelectric studies, it has already enabled the appearance of thermoelectrics based on silicon with a zT of 1 at low temperatures of 200 K [30], where the bulk counterpart has yet to exceed 0.01 at any temperature. The use of porous anodic alumina (PAA) [Figure 1.12 (a)] or carbon nanotubes as templates for these wires is a recent development for thermoelectrics, still under heavy scrutiny but showing very promising results for low cost, high zT production processes. The possibility of creating large arrays of PAA filled with, for example Bi_2Te_3, would provide much higher zT than the bulk counterpart due to the higher number of interfaces. Another possible approach is that of malleable thermoelectrics using these arrays of nanowires in PAA, which would improve even further the number of possible markets this technology can reach [31-33]. The possibilities of these structures for thermoelectrics are truthfully immense and many other materials, which were presented as bad thermoelectrics, have already been predicted to show zT's 1000 times bigger than their bulk counterpart when reduced to the nanoscale [Figure 1.10] [28, 29]. In order to reach the maximum zT possible, PAA has been heavily applied in the fabrication processes of thermoelectric materials, since it presents the perfect thermal transport properties for a template [Figure 1.12]. The most recent developments in this technology have been around Bi_2Te_3

nanowires [34-39] [Figure 1.12 (b) and (c)], with reports that the zT's of these wires are already as high as the bulk's but with much lower costs. It is also important to notice that these values are for wires far too wide to bring about the predicted zT increase as in the wires presented in Figure 1.9. This means that further developments will allow the fabrication of thinner wires, which could increase the zT values to a new record.

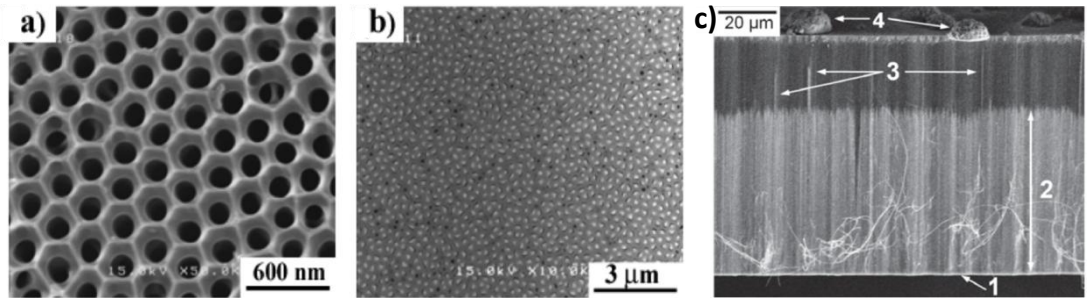

Figure 1.12 Scanning electron microscopy images of (a) highly ordered nanopores in PAA, [(b) and (c)] Bi_2Te_3 nanowire array in a PAA template: (b) top [39] and (c) cross-sectional [34] views. The numbers in (c) correspond to: 1) bottom gold layer, 2) nanowires, 3) nanowires with outstanding length, and 4) hemispherical overgrowth on top of the membrane.

1.6 Motivation and objectives

Boosted by the search of more efficient thermoelectric devices, easy, cheap and scalable production of nanostructured materials has been the main aim of the most recent developments in this technology. In accordance with this line, this work has the following objectives:

I. Production of both p and n type thin films of Bi_2Te_3 using the electrodeposition process.

II. Development of Bi_2Te_3 nanowires using a PAA template.

III. Production of a microgenerator based on the results of the thin films and nanowires.

This thesis is devoted to the development of nanostructures (2D and 1D) of thermoelectric materials based on Bi_2Te_3 compounds using electrodeposition technique. On the thin films, the study of best electrodeposition parameters, namely influence of potential and time are addressed paying attention on the effect on morphological, chemical (semiconductor type) and atomic structure. Moreover, a system for the measurement of the Seebeck coefficient of thin films are also an objective of the present work.

On 1D structures, based on the results obtained on the thin films, by using alumina porous template, nanowires of Bi_2Te_3 will be developed. Finally, by using lithography process, the development/design of a thermoelectric prototype will be also discussed in this thesis.

Finally, it is expected that with the results obtained in the present thesis will open new avenues on the development of cost-effective and environmentally friendly rigid and flexible thermoelectric micro/nanodevices for power generation.

Chapter 2

Materials preparation and experimental set-ups

2.1 Introduction

In this chapter a resumed view over the electrodeposition process of Bi_2Te_3 thin films, fabrication of porous anodic alumina (PAA) membranes and nanowires growth assisted by these nanoporous templates will be described. Additionally, a brief description of the techniques used for the morphological, chemical and structural characterization of the fabricated nanomaterials will be presented, namely X-ray diffraction (XRD), scanning electron microscopy (SEM), energy-dispersive X-ray spectroscopy (EDS) and profilometry. On transport properties, the electrical resistivity of the thin film using the 4 contact method will be described. The detailed development of the Seebeck coefficient measurement apparatus implemented during this thesis will be presented. In order to develop the first prototypes of microdevices, clean room facilities were also used, namely the optimization of the litography process for direct writing, the use of this same direct writing and electron beam deposition. Finally, a benchmark set-up for the testing of the performance of the microgenerators fabricated under the present thesis will be shown.

2.2 Fabrication of nanomaterials

2.2.1 Electrodeposition process

Three different electrodeposition types have been commonly used for the electrodeposition of Bi_2Te_3: potentiostatic deposition, potential-pulsed deposition and constant potential and constant current in pulses method [40,43].

Potentiostatic three electrode cell procedure was picked as the main deposition process due to its very high growth rates, easy reproducibility in the industrial level, very simple apparatus and experimental procedure. This technique [Figure 2.1] is connected to the need to create a stable, fully reproducible process able to properly study the behaviour of the material deposited at the working electrode while monitoring the current and potential during the growth process. At the start of this process it is necessary to perturb the system by breaking equilibrium, which is done by applying a potential in the working electrode, where the sample is connected. Since the potential of the cell needs to be measured between the working electrode and another electrode (eq. (2.1)), a well known, constant potential is paramount for the other electrode, to diminish variations and errors in the system [44]. This other electrode is entitled the reference electrode and, in our case, is Ag/AgCl (in 4M KCl) to serve as a constant reference (0.197 V vs standard hydrogen electrode; SHE).

$$\Delta V_{cell} = V_{WE} - V_{RE} \quad (2.1)$$

Furthermore, the use of one single electrode for the measurement of both the current and potential in the cell would mean a greater amount of error, since large currents passing through an electrode might change its potential. This is solved by using a third electrode, a counter electrode which is then used to measure the deposition current separately from the potential to ensure the most stable and repeatable process possible [44]. This electrode needs to be composed of an inert material in order to keep the solution pure of any parasitic effects. In our case this is done by a Pt mesh which closes the circuit for the current measurement. Due to the necessity of a conductive material in the working electrode for the initial creation of this current, the working electrode must always be composed of a conductive or semiconductive layer.

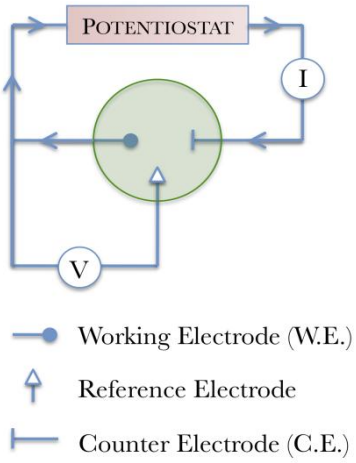

Figure 2.1 Three electrode cell method schematic [45].

Since the used reference electrode is Ag/AgCl, all the potentials presented in this work are in reference to it and are all presented in modulus. This point is vital to understand the effects of the electrodeposition potential and to address the relations between it and several physical properties of the samples.

2.2.2 Thin film preparation

For the electrodeposition of thin films, the three electrode set-up visible in Figure 2.2, was used. The apparatus was based on the suspension of the working electrode into the electrolyte due to the need to maximize all samples length and to simplify even further the deposition process. The thin films were deposited in a common 100 ml beaker filled with 80 ml of electrolyte. The reference electrode was closely packed to the sample and finally a Pt mesh was placed on the opposite side of the reference electrode. The temperature of the room was kept constant (23 ºC) throughout the entire process. The applied potential and measured current were monitored using a remote controlled sourcemeter.

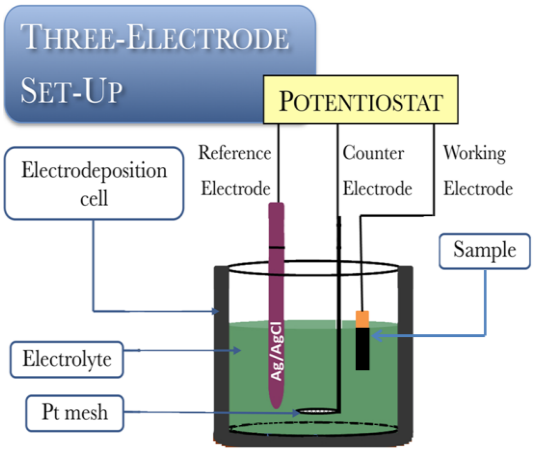

Figure 2.2 Three electrode set-up used for the electrodeposition of thin film structures, adapted from [45].

In search for the best parameters possible for the stable growth of free standing Bi_2Te_3 thin films, several different substrates, electrodeposition potentials and deposition lengths have been tested. A preliminary study on Cu stripes as working electrodes was conducted. These stripes were traditionally of 1.5 x 1.5 cm^2, flexible and with 99.9% purity. Prior to the deposition process, these were cleaned in acetone, ethanol and deionised water for 5-10 minutes, in an ultrasounds bath. At a second stage, silicon wafers (cleaned by the same method) were also used as substrates, with a sputtered Au layer of about 50-100 nm on top to serve as the working electrode. Due to some limitations found during the deposition process on these substrates, several other materials and electrical contacts were also tested. With different success rates, ITO (Indium tin oxide), silicon, glass and PMMA (Poly(methyl methacrylate)) substrates were used. Of these, ITO, silicon and glass had a Cu layer of 50-75 nm thick evaporated on top to serve as an electrical contact. Other metallic contacts were also tested, such as Al, Al/Cu, Ti, Ti/Cu, Cr, Cr/Cu, Fe, Au and Pt. These tests allowed us to better understand the materials' ability to withstand the solution acidity and HNO_3 concentration, which traditionally attacks conductors such as Cu and Fe [46].

Four different electrolytes have been tested all to tackle different needs of these structures, such as the creation of p-type and n-type pillars, more stable growth, solution aggressiveness and many other properties. The first one was composed of 10 mM Bi^{3+} and 15 mM $HTeO^{2+}$ ions in 1 M HNO_3 diluted in deionised water [42]. This was done by dissolving measurable amounts of bismuth(III)-nitrate pentahydrate $Bi(NO_3)_3 \cdot 5H_2O$ (Sigma–Aldrich) and pure Te powder (99.999%) in concentrated nitric acid. The chemical reaction, for the formation of the thin film from this acidic solution is:

$$3HTeO_2^+ + 9H^+ + 18e^- + 2Bi^{3+} \rightarrow Bi_2Te_3 + 6H_2O \qquad (2.2)$$

Bismuth telluride is insoluble in dilute nitric acid, which means that the higher rate of reduction of Te^{2-} combined with the lower reduction rate of Bi^{3+} will precipitate Bi_2Te_3 on the electrode surface [42].

The second electrolyte was very similar to the first one, with a higher concentration of Bi^{3+} by doubling the amount of bismuth(III)-nitrate pentahydrate $Bi(NO_3)_3 \cdot 5H_2O$ (Sigma–Aldrich) in the solution and

maintaining the amount of all the other reagents, having been nominated as the p-type electrolyte. The third electrolyte had the exact same concentrations of reagents in deionised water as the first one but with the addition of 40%, in volume, of ethylene glycol (EG). This is entitled as the 40%EG n-type electrolyte. The last one had the same concentrations as of the second type but with 40% total volume of EG and was designated as the 40%EG p-type electrolyte. The use of these last two electrolyes was based on recent reports, by Li *et al.* [47] where this compound actively assisted in the improvement of the deposition of these materials, by raising their adhesion to the conducting layer, improving film homogeneity and possibly enhancing the thickness limit. Series of five to seven samples were used, with electrodeposition potentials between 0.15 V and 0.75 V. Typical depositions lasted for 15 min up to 2 h. All depositions were conducted at room temperature in unstirred solutions.

2.2.3 Porous anodic alumina templates

The fabrication of PAA [48-52] requires high purity aluminium foils (99.999% purity), cut in squares of 1.5 x 1.5 cm^2 in the case of this work. These are cleaned in acetone, pressed and then immersed in ethanol in an ultrasonic bath for 10 min. This is then followed by an electropolishing process which is used to smoothen the surface of the Al foils and remove any impurities or oxidation. This process is important to obtain a highly homogeneous membrane. The electropolishing solution is composed of 25% percloric acid ($HClO_4$) and 75% ethanol and the process lasted for 2 min at 20 V at a temperature below 8ºC.

This is followed by a first anodization which varied between 6-24 h in a solution with 0.3 M oxalic acid ($H_2C_2O_4$) at 40 V and a temperature around 4°C. During this step, a nanoporous alumina layer is formed on top of the Al foil, creating an organized array of pits at the Al surface, which will serve as nucleation points for the nanopores growth during a second anodization process, thus forming a fully organized and structured porous membrane. The need for a second anodization [53] arises due to a poor organization of nanopores after only one of these steps, as is seen in Figure 2.3 (a). It is observed that in one step the template is highly undesired due to defects, disorder in the anodization process or the need to have a stable pores distribution throughout the entire membrane. This is visible in Figure 2.3 (b) that most of these defects are corrected after doing the second anodization. In order to do the second anodization, one first needs to remove the alumina layer of the first anodization, which was done in an aqueous solution of 0.2 M H_2CrO_4 and 0.4 M H_3PO_4 at 60°C for around 5-20 h [52]. Second anodizations were then performed for 40 h with the same solution and temperature as in the first anodization, in order to create a PAA with a pore diameter of around 35 nm, an interpore distance of 105 nm and a thickness of about 100 μm. After this process, the alumina template is complete and further processes are done depending on the required conditions for future applications.

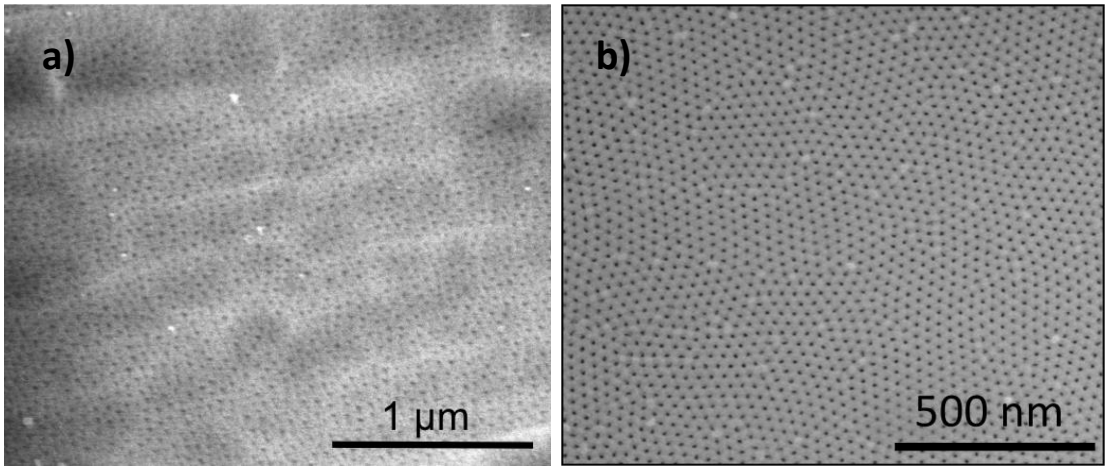

Figure 2.3 SEM top image of the result on the PAA organization after (a) only the first and (b) the second anodization [45].

2.2.4 Electrodeposition of nanowires

After the creation of the alumina template it is then necessary to clear the bottom pores. This is done in order to deposit a conductor for the potentiostatic deposition. This means that the bottom part of the PAA needs to be cleared of aluminium first and then cleared of the oxide layer which is blocking these bottom pores. The chemical etching of the Al foil is done in an aqueous solution of 0.2 M $CuCl_2$ and 4.1 M HCl at room temperature for about 10 min. The alumina barrier present is then removed by chemical etching in a 0.5 M H_3PO_4 solution at 40°C for 30 minutes [52]. This process enlarges the final pore diameter to around 50-60 nm. Finally, a 50 to 100 nm Au layer was sputtered at the bottom of the opened pores to serve as the working electrode in the potentiostatic deposition.

The deposition set-up, seen in Figure 2.4, is quite similar to the thin film process but, due to the fragility of the PAA and to obtain the best deposition possible, the membrane was wedged between a Teflon container with a hole with 1 cm of diameter and a Cu plate. This was tightly shut to guarantee that no solution was leaked during the deposition process and to guarantee maximum electrical contact between the Cu plate and the membrane. The reference electrode was then placed very closely to the membrane in order to guarantee that the correct potential was applied. Finally a Pt mesh is used to close the circuit for the current measurement. The electrolyte temperature was kept constant throughout the entire process.

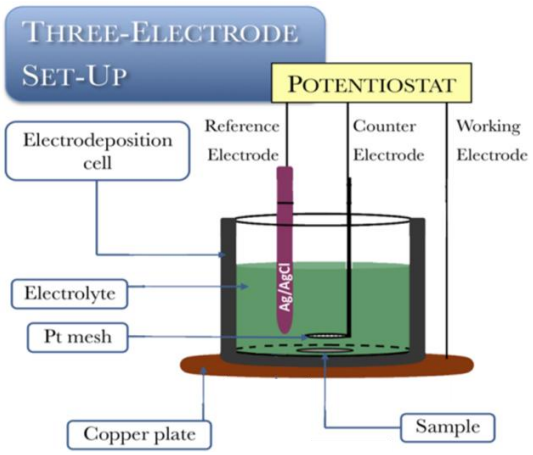

Figure 2.4 Three electrode set-up used for the electrodeposition of nanowires, adapted from [45].

2.3 Characterization techniques

2.3.1 Profilometer

In order to define a sample's roughness, defects and thickness, a profilometer Dektak XT, Bruker from CEMUP-MN facilities was used. This technique traditionally uses a diamond stylus which is kept in contact with the sample by applying a defined contact force, connected to a very precise and sensitive spring. The system guarantees that the defined force does not vary, which translates in the stylus moving vertically with every variation on the sample's surface giving rise to a mapping of this surface's roughness and defects. By using this principle on a previously prepared discontinuity in the sample, it is possible to define a sample's thickness [54].

2.3.2 SEM/EDS analysis

A scanning electron microscope (SEM) is a technique based on the use of a highly focused electron beam, with a spot of a few nm, accelerated by a 10 to 20 kV potential to study a sample's morphology. This beam will interact in several different ways with the sample creating back scattered and secondary electrons, utilized to create an image of the sample, characteristic X-rays used in EDS scans and Auger electrons [55].

Secondary electrons are the result of inelastic interactions (low energy) between the electron beam and the sample's surface atoms. These are the most commonly used source in SEM imaging when studying the surface topography due to being the major result of the beam's interaction and for having the highest spatial resolution and low sample penetration.

Back scattered electrons are the result of the elastic collision between the accelerated electron's and the surface of the material. They have a very high energy but occur in a much smaller scale. These present the best depth contrast, have a larger area of production in the sample and have a great advantage of showing an atomic number contrast which helps to better distinguish between two distinct chemical composition and thus allowing to distinguish for instance the nanowires produced in an alumina template.

Finally, the characteristic X-rays and Auger electrons appear in the cases where the beam interacts with the inner levels of the atom, expelling one of its inner electrons. This is then followed by the transition of a higher level electron to the vacant position with the release of a photon with a well established energy. This is finally followed by one of two events: either the photon is absorbed by a higher level electron which gets ejected from the atom, an Auger electron, or the emission of X-rays occurs. These X-rays' energy are well quantified and are characteristic to every atom which allows for good understanding of the elements present as well as their quantification in the sample. This is what is being measured in the energy-dispersive X-ray spectroscopy (EDS) study [Figure 2.5] [55]. This technique has a typical error of $\pm 2\%$ in stoichiometry measurements at the best conditions, degrading quickly with roughness.

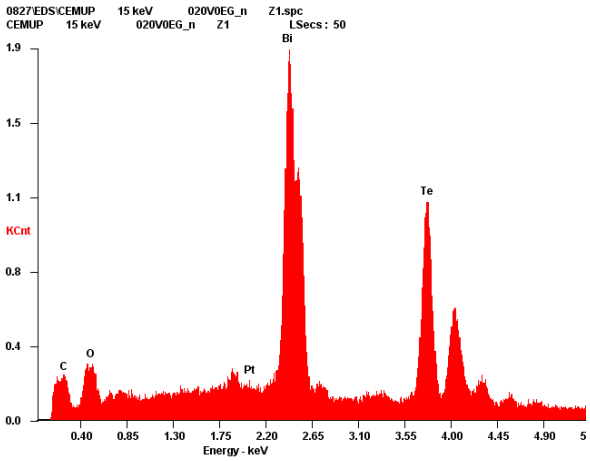

Figure 2.5 Typical EDS result of Bi_2Te_3 samples, in this particular case, on a Pt substrate.

These techniques were used in CEMUP's facilities, having been used the model FEI Quanta 400FEG ESEM/EDAX Genesis X4M and in the "UNIDADE DE MICROSCOPIA ELETRÓNICA" of Vila-Real the device FEI Quanta 400, W filament; EDS/EDX from EDAX.

2.3.3 X-ray diffraction analysis

To study the crystallinity of the nanostructures prepared, X-ray diffraction (XRD) was thoroughly used in this work. In summary, the XRD principle arises from bombarding a sample with X-ray radiation which is elastically scattered by the atoms in the sample. From this scattering, it is possible to analyse the crystallinity of the sample (low crystallinity leads to absence of peaks reflections due to the random direction of these X-rays) [55]. In the case of crystal structures these scattered X-rays will show two kinds of interference: in most directions it will be destructive but, due to the regularity of the crystal in well defined situations the interference will be constructive, which translates in the appearance of peaks of intensity for these specific situations. This is connected to Bragg's law (2.3) [55]

$$2d\sin(\theta) = n\lambda \tag{2.3}$$

Where *d* is the spacing between a crystal's atomic layers and λ is the X-ray's wavelength. The information taken from an XRD analysis allows the understanding of what phases (space group) are present in the sample. With that purpose, it was used the Bragg Brentano configuration [56]. Furthermore, from the shape/size of the peaks reflections we could extract information about the crystalite size, using the Debye-Scherrer formula [56]:

$$\tau = \frac{K\lambda}{\beta\cos\theta} \tag{2.4}$$

Where τ is the mean size of the crystallite, K is a dimensionless shape factor which has a value very close to unity, λ is the wavelength of the X-ray, β line broadening at half maximum intensity and θ is the Bragg angle.

Finally by using fullprof software [57], namely the Le bail fit, it could be extracted the volume of the unit cell. This measurement system is completely non-destructive and has very high penetrations depths, providing a good understanding of the sample's characteristics instead of only their surface, which could be quite different from the rest of the studied material.

This technique was used in IFIMUP-IN's facilities and the device was a Siemens D5000X-ray difractometer and in the "UNIDADE DE MICROSCOPIA ELETRÓNICA" of Vila-Real the device PANalytical MPD (omega/2teta) with X'Celerator detector and secondary monochromator.

2.4 Conductive layer deposition methods

2.4.1 Sputtering

The used sputtering was BOC EDWARDS Scancoat Six and was applied in this work to deposit thin layers of Au. The sputtering process is mainly used for thin film production or etching and consists of a vacuum procedure where a cloud of ions formed from a noble gas (Argon in the sputtering method used in this work) are accelerated against a previously picked target by a potential present in the chamber. This will create a cascade of collisions in the target which, once they reach the surface of the target with an higher energy than that of the surface binding energy of the material, will expel it from the target. This is, thus, the exchange of momentum between the accelerated ions and the atoms of the element to deposit. The element expelled this way will deposit over any area under the target, including the previously prepared substrates. In the case of this thesis, a magnetron sputtering was used, which has a higher density of deposited films. This is connected to a higher power density focused in shorter impulses. This process allows for a great control over thin film thickness, having shown a successful controlled deposition of 50 nm of Au. This technique has the major advantage of easily depositing high vaporization materials since it is based on another completely different effect [55].

2.4.2 Thermal evaporation

This technique was used for both the deposition of Al, Cu, Cr, Al seed layer with a thicker layer of Cu and Cr seed layer with thicker layer of Cu. A conductive filament, typically of (W), is used to heat up a predetermined material to its evaporation temperature whence the material will evaporate and condense in an area directly in the line of sight of the process which has a prepared substrate. A vacuum of about 3×10^{-6} Torr (~4×10^{-4}Pa) needs to be established to guarantee that only the desired evaporated material reaches the substrate without any significant contamination. This process has a high control over the rate of deposition [58].

The used facilities for this process were the Unidade de Micro e Nanofabricação - MNTEC and the equipment was an homemade model with an Edward vacuum pump.

2.4.3 Electron beam deposition

This technique was used for the deposition of Fe, Ti, Cu and a Ti seed layer followed by a thicker Cu layer. This technique is based on thermal process (similar to the previous one) but where a filament is heated enough for the thermal energy of the electrons to be higher than their binding energy. This will release the electrons which are then accelerated by the application of a potential against the material which has to be evaporated. This acceleration occurs due to the use of a high potential between the filament and the container which has the material up to 30 kV. These electrons will hit the material and rapidly lose their energy, mostly in the form of thermal energy into the sample. The conversion of this electron kinetic energy into thermal energy reaches values as high as 85% for potentials as high as 25 kV [59]. The evaporated material will then deposit everywhere in a defined cone where the desired substrate will be present. The used facilities for this process were the Unidade de Micro e Nanofabricação - MNTEC and the equipment was Auto 306, Edwards.

2.5 Direct laser writing

This technique, used mainly for the first prototype shown in this work, is based on the use of a highly focused laser beam to hit a photosensitive polymer, traditionally called photoresist, in order to draw a predetermined structure and pattern in this material. This technique has the advantage of having very high resolutions, in the order of 1 μm and is a versatile technology due to the ability to create lithography masks which are used as moulds to create a high number of a certain structure without adding to many costs. A S1818 photoresist was used as a supporting structure for the devices created using this method, having been hard baked for 1 min after being in the spinner at 4000 rpm for 30 seconds. The used facilities for this process were the Unidade de Micro e Nanofabricação - MNTEC and the equipment was laser uPG101, Heidelberg.

2.6 Thermoelectric properties

2.6.1 Seebeck coefficient measurement

In order to categorize the quality of the thermoelectric properties of the thin films, the study of the Seebeck coefficient was developed during this thesis. The Seebeck coefficient is obtained from the linear relation between the measured potential and the gradient of temperature on the sample, seen in the equation (1.1):

$$\mathbf{S} = \frac{\mathbf{\Delta V}}{\mathbf{\Delta T}} - \mathbf{S_{wire}} \tag{2.5}$$

where the S_{wire} is the characteristic Seebeck value of the electrical contact for the measurement of the ΔV relative to Pt (the used wire with low Seebeck effect). In order to perform accurate measurements, a good control over thermal loss centres are vital. This is made by establishing a proper and stable

temperature gradient, thus guaranteeing that there are no types of thermal parasitic effects, and also by giving a special attention to any electrical leakage or high thermal losses during the measurement.

The measurement set-up used for this process is represented in Figure 2.6. A gradient of temperature is first applied by heating one of the Cu support towers, and simultaneously measured between the two electrically isolated Cu towers, using a Type K differential Thermocouple automatically controlled by a LakeShore 331 Temperature controller. When this gradient reaches a stable value, an Agilent 34420A 7 1/2 nanoVoltmeter is used to measure the actual temperature gradient present in the sample, via the usage of another independent Type K thermocouple which is electrically isolated from the sample. After both of the temperature gradients reach a stable period, another Agilent 34420A 7 1/2 is used to measure the actual electrical potential in the sample, which arises from the Seebeck effect. This process is repeated several times with rising temperature gradients.

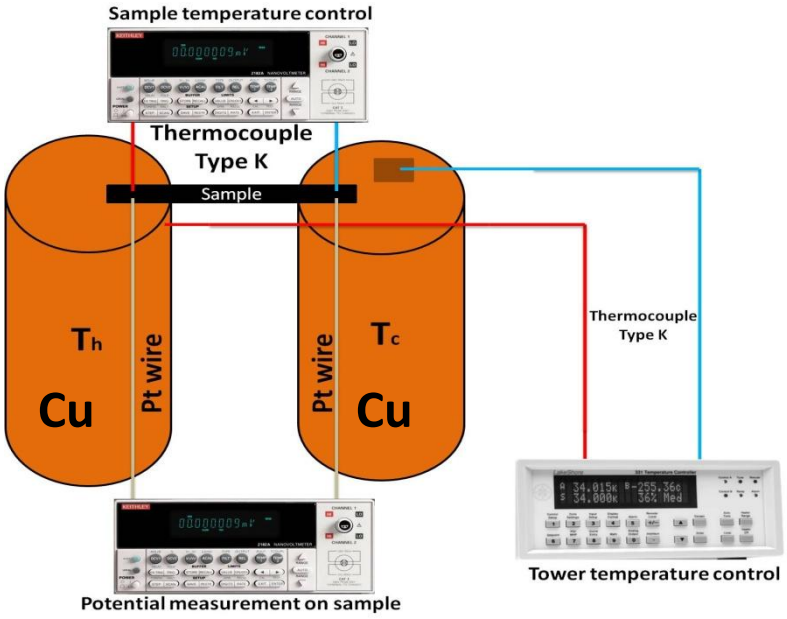

Figure 2.6 Schematic representation of the Seebeck coefficient measurement apparatus created for this project.

Control measurements were done on Fe samples as a reference material to prove the quality of the measurement set-up assembled. Figure 2.7 (a) shows the experimental values obtained, and the respective linear fit used for the estimation of the Seebeck coefficient. The value obtained is of around 21.9 μV/K, which is fairly near to the theoretical predicted value of 18.9 μV/K [60].The small difference between the theoretical value and the measured one (around 3 μV/K) might be explained as possible losses or interferences in the measurement system or possible Fe oxidation. This value represents an error of about 15% which is quite acceptable. A second measurement was made on a Cu stripe used as the conductive layer for the Bi_2Te_3 electrodeposited samples [Figure 2.7 (b)]. The results obtained (around 7.0 μV/K), are very similar to the theoretical ones of 6.5 μV/K [61] with a difference of only 1 μV/K, which corresponds again to an error of about 15%. This further confirms the quality and reproducibility of the process, and will allow us to make the respective corrections in future measurements.

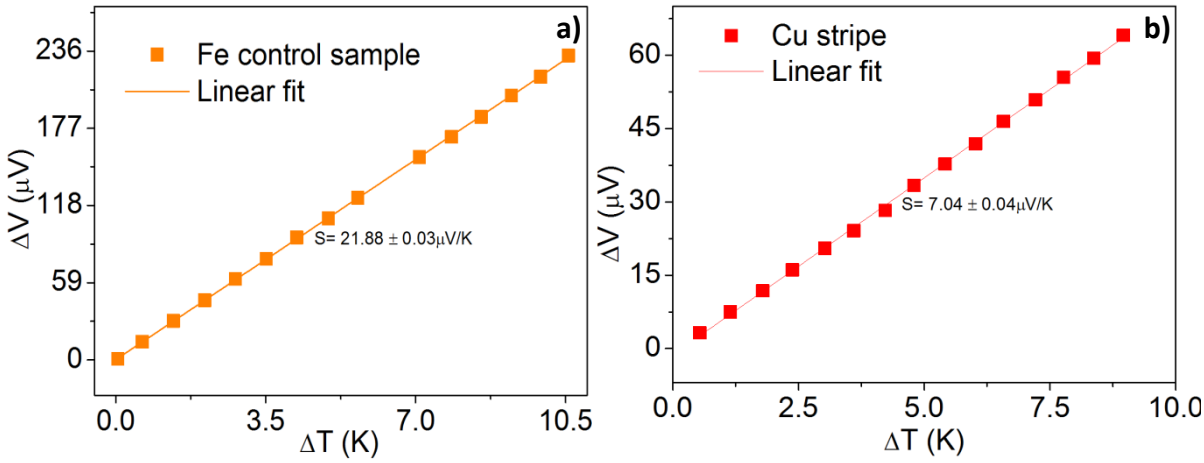

Figure 2.7 Seebeck coefficient measurement of (a) a pure iron sample and (b) a copper stripe for calibration.

2.7 Electrical resistivity

Four terminal sensing is a more common measurement system of electrical resistance. In this system, four conductive wires are connected to the sample, as seen in Figure 2.8, to read the potential between the wires 2 and 3 and current between 1 and 4. This technique is highly accurate and is based on the fact that if a single pair of wires was used, the reading would have a source of error which is their own resistance. This is connected to the fact that the reading wires would be the same as the ones used to apply the reading signal, which would translate in a contribution from their resistance. This is not the case by using a secondary pair of wires which will serve to supply current to the sample, creating a low impedance circuit that almost totally negates the current that passes in the measurement connections (wires 2 and 3). This completely clears the contribution of this pair, reading in this way exclusively the sample.

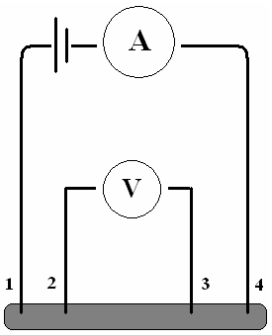

Figure 2.8 Four terminal sensing diagram. The wires 1 and 4 are used for current injection while the wires 2 and 3 are used for potential readings.

2.8 Benchmark set-up for thermoelectric devices

In order to study the output of the first prototypes based on the thermoelectric effect, a simple measurement apparatus was built [Figure 2.9]. The sample in study was wedged between two Peltier devices, where the top one was used to cool the top part of the sample and the bottom device was

used as a heater for the bottom of the sample. This was done in order to submit the sample to a gradient of temperature and, therefore, be able to properly read its output. We connected the nanoVoltmeter to both the top and bottom of the prototype in order to read the potential that was being created by this effect. A study was conducted where the gradient was grown linearly and each subsequent potential was registered, having in this way a knowledge of the possible potential that might be retrieved from these samples.

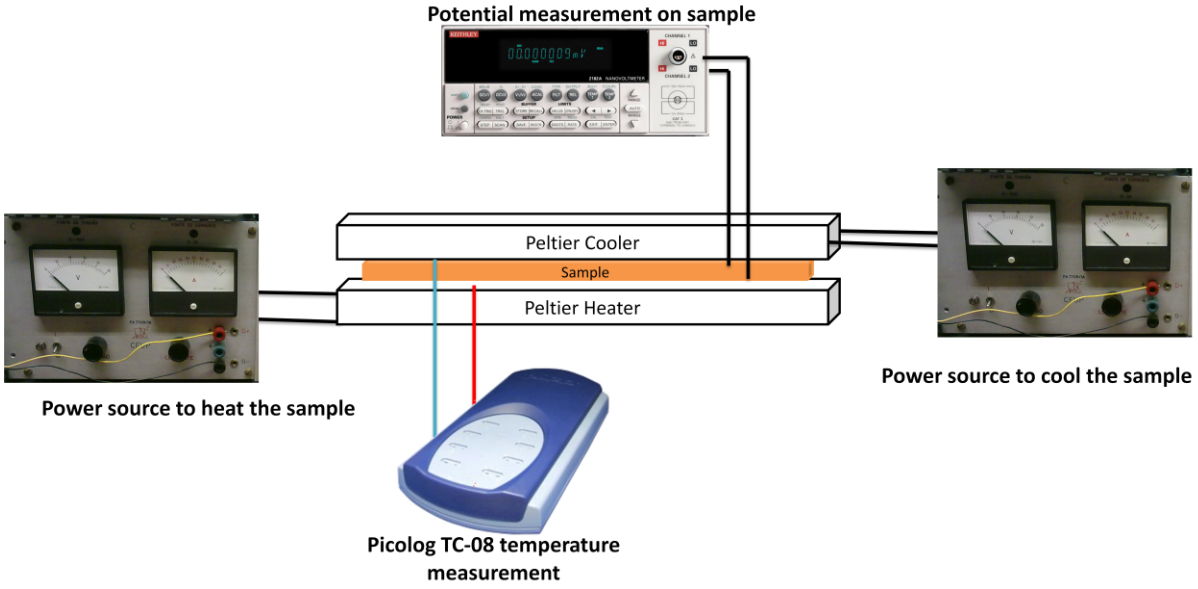

Figure 2.9 Benchmark set-up for thermoelectric devices.

Chapter 3
Electrodeposition of Bi_2Te_3 thin films

3.1 Introduction

In chapter 1 it was highlighted the importance of the development of thermoelectric nanostructures where thin films growth is crucial for the effective increase of zT. Moreover, the industrialization of these structures requires specific characteristics: low material content and equipment investments, high deposition rates, highly reproducible processes and low sample variation. In order to tackle all these requirements, the electrodeposition of Bi_2Te_3 thin films has been one of the main focuses in this work, due to this material's naturally high thermoelectric properties, the use of low production costs and the industrial capabilities of electrodeposition.

Due to the increased demand for the best parameters to produce high quality thermoelectric materials by electrodeposition, several different approaches have been addressed: varying electrodeposition potential and deposition time, tuning the electrolyte composition and concentration and testing several different substrates. The main aim of this research was to reach a complete stoichiometry control in order to produce both p-type and n-type Bi_2Te_3 thin films, thus impelling the production of microgenerators based on this principle. Typical electrodeposition curves are presented in order to categorize the growth patterns of the different samples. Description of the morphological, structural and stoichiometry of the resulting samples are also shown. A thorough study on the effect of the electrodeposition potential on the crystallinity, preferential growth direction and general quality of the samples is also presented. Finally, Seebeck coefficient and resistivity measurements have been conducted in some of the samples in order to study their thermoelectric properties.

3.2 Results and discussion

3.2.1 Electrodeposition analysis

An important factor in the electrodeposition method to achieve high quality thin films and reproducibility is the choice of substrates to be used. Several substrates were tested [Chapter 2.2.2], being the substrates of Si with a thin layer of Pt (to insure electrical contact) [62] on top, the ones that presented the highest reproducibility (more than 90% of success).

The deposition curves during the electrodeposition process for the Pt layer substrate can be seen in Figure 3.1. There is relevant information to be extracted from the these curves since they allow to follow the rates of deposition as well as an overall growth of the thin films without using expensive equipment inaccessible for industry such as SEM or XRD. Analysing the curves obtained it can be seen that the process initiates with a significant drop in electrodeposition current followed by a quick constant stabilization. This behaviour is related to the covering of the first Bi_2Te_3 layers on the top of Pt increasing the resistivity of the electrode due to highest resistivity of Bi_2Te_3 when compared with Pt.

After the existence of a Bi_2Te_3 layer over the Pt layer, the current tends to stabilize since the resistance of the electrode will remain constant.

Using the typical electrodeposition process, there is an issue related with the adhesion of the material electrodeposited to the Pt electrode. In order to solve this issue, in literature can be found [40] that by adding in the solution 40% ethylene glycol the adhesion is improved, which was confirmed in the present work. Concerning the electrodeposition current curves for the samples prepared with 40% of EG there is a clear systematic decrease of the overall deposition current between the EG free electrolytes [Figure 3.1(a) and (c)] and the 40% EG electrolytes [Figure 3.1(b) and (d)], which indicates a much lower rate of deposition when using the latter electrolyte. These two facts might be connected with a much lower concentration of Bi and Te ions in the solution, which might strongly inhibit the deposition of these materials.

The values of these deposition currents lack high precision, connected to small deviations of the effective deposition area of the sample. These small deviations connected with irregular forms have hindered a more systematic measurement of these areas. This is very clear in Figure 3.2, where using the same applied potential for different times, lead to different stable current values that can only be explained by size of subtract. Therefore, during the thin films growth only the deposition current transients will be presented.

This could not still explain the overall reduction seen in Figure 3.1(b) and (d) since this is a consistent decrease in current in all of the samples subjected to the EG rich electrolytes which could not be simply explained by these small deviations in sample area. It is also possible to visualize the appearance of what seems like a periodic noise in the deposition current in some of the samples [mainly in Figure 3.2] which arises from an interference on one of potential sources, seen in the difference between the three “noisy” curves and the two “smooth” ones was the use of a difference sourcemeter.

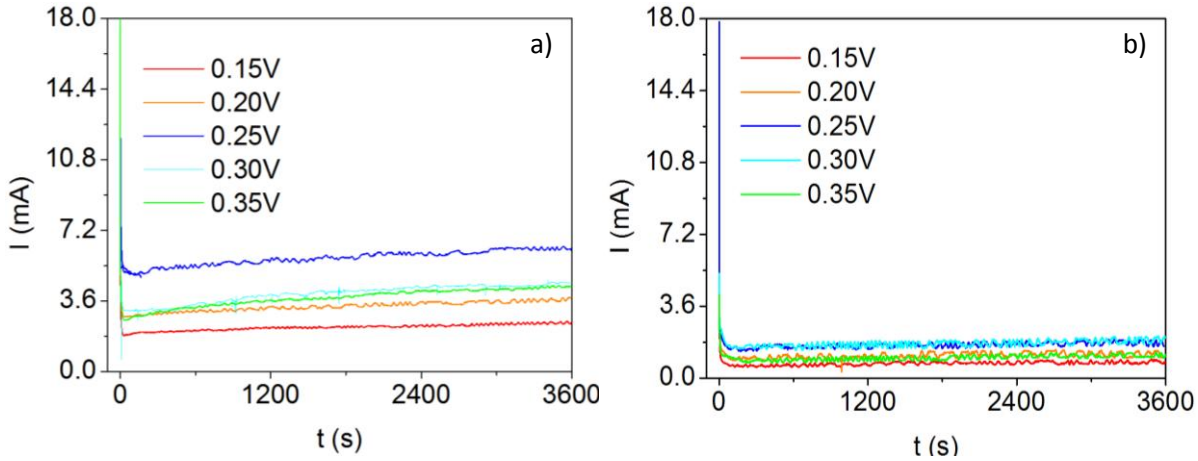

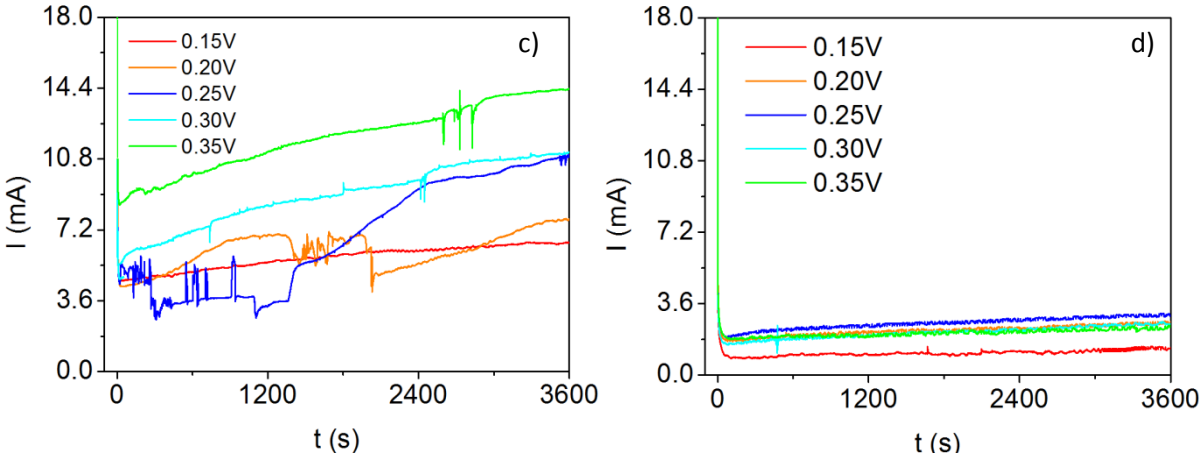

Figure 3.1. Current transients measured during the deposition process of the thin films on a Pt covered Si substrate using different electrolytes: (a) n-type, (b) 40%EG n-type, (c) p-type and (d) 40%EG p-type.

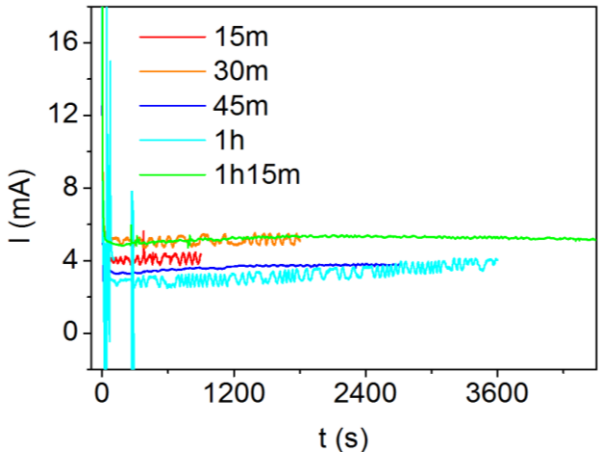

Figure 3.2. Deposition curves of the samples electrodeposited at 0.25 V, for different times (15m, 30m, 45m, 1h and 1h15m), on Cu stripes using the n-type electrolyte.

Moreover, from Figure 3.1 and Figure 3.2 it outcomes that there is not much difference between the deposition curves when using a Si+Pt substrate or a Cu stripe, which might indicate that both deposit occur in similar ways. In case of using Cr as seed layer and Cu as electrical contacts (Cr+Cu) on the top of glass substrate, a much lower deposition current (10 times lower at the same deposition potential) is achieved [Figure 3.3 a)]. In case of using an Al seed layer and Cu as electrical contact (Al+Cu), the electrical current value are near the ones present in Pt or Cu stripes, but the deposition stops abruptly near the 40th minute (second 2400) when it should go on for 20 more minutes (3600 seconds). In fact, it was observed that the Cu layer completely peeled off the substrate and broke the electrical contact. This happens due to an aggressive attack of the 0% EG electrolyte on the Al and Cu layers, which may be due to several factors: the very low pH of the electrolyte used (~1) and the high concentration of HNO_3. HNO_3 has a very high aggressiveness on conducting materials [46] and possible reduction reactions that might occur simultaneously with the deposition process, since the degradation of the surface was seen optically to highly accelerate with any applied potential. The peaks that appear on the current transients throughout the whole deposition process are due to possible cracks/discontinuities formations on the conducting layer that appear during the process thus

exposing new areas of Cu where no deposition had yet occurred. This explains the new peaks of deposition current seen in Figure 3.3 throughout the duration of the process. Several other materials studied in this work suffer of this effect, with the most extreme of all being iron, with a maximum deposition time of 40 to 50 seconds before it peels off completely due to a particularly strong reaction with electrolyte. Another observed effect that highly influences the deposition process is the electrical resistance of the metallic contact. If the working electrode shows an electrical resistance over 10 Ω, the deposition is highly inhibited, if not totally inhibited. This is especially visible in Figure 3.3 (c) where a deposition in the conductive side of ITO is shown. With a measured resistance of about 100 Ω not only is the deposition highly unstable (as seen by the high variations in the deposition current), but at about the 13th minute the deposition abruptly diminishes and near the 20th minute it stops completely [Figure 3.3]. By analysing optically the sample deposited, it was possible to observe that a thicker layer was depositing on the limit between the electrolyte and air, which ended up opening the circuit after about 20 min (1200 s). Even before this abrupt cut on the deposition pattern, the growth throughout the sample was also found to be highly inhomogeneous and unrepeatable.

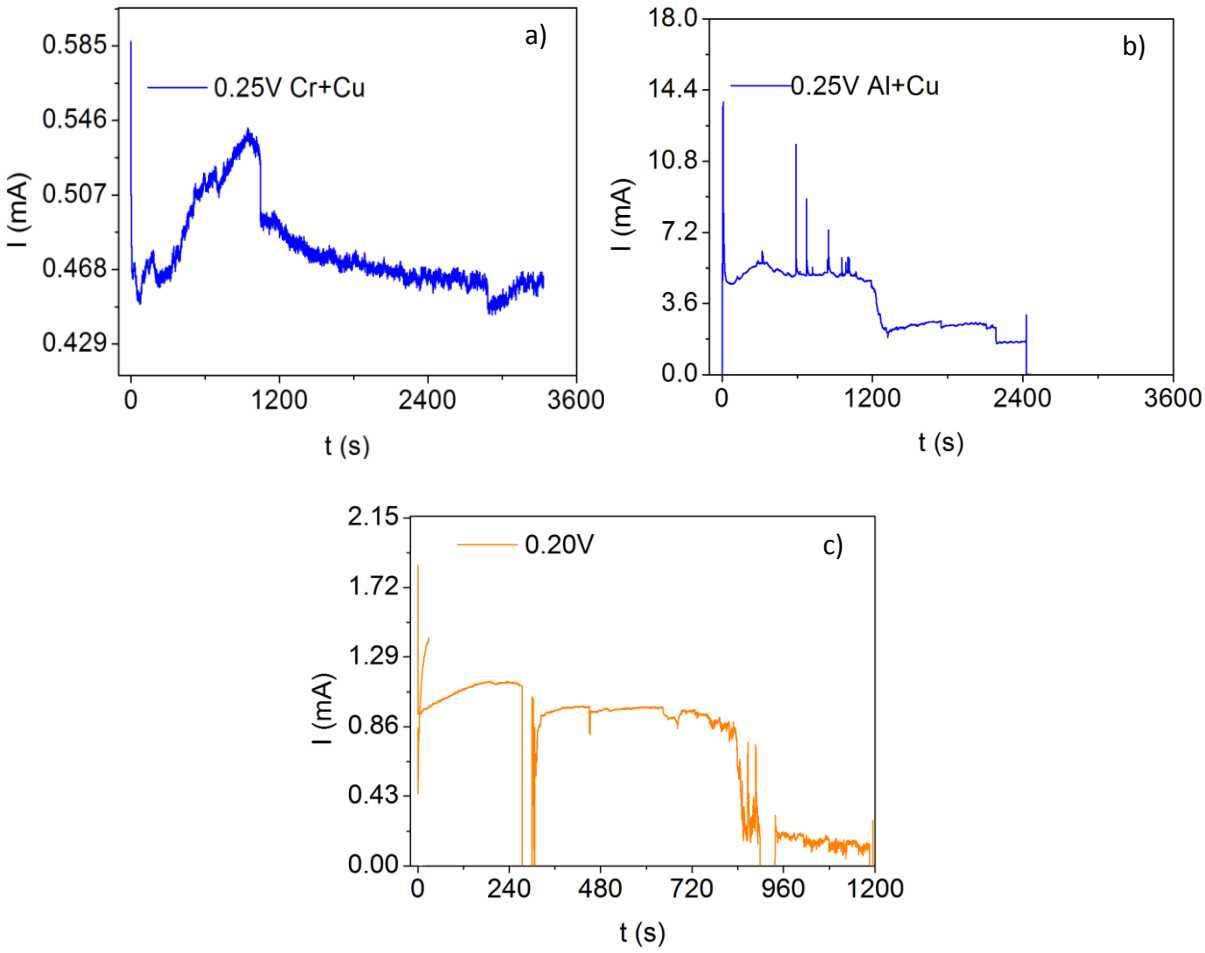

Figure 3.3. Deposition curves at fixed potential on different substrates such as (a) glass with a Cr seed layer covered with 75 nm copper thin film, (b) Al seed layer with 75 nm copper and (c) ITO substrate.

3.2.2 N type electrolytes results

The construction of a thermoelectric module requires the use of two types of semiconductors (see chapter 1), p type and n type, meaning there was a strong need to develop high efficient n-type Bi_2Te_3 thin films. Bulk Bi_2Te_3 shows the highest room temperature zT for any kind of thermoelectric and is normally found as a n-type semicondutor [Figure 1.3]. As abovementioned, two electrolytes will be used: one EG free and the other with 40% EG volume, where the improved thin film adhesion was already mentioned. Nevertheless, one should also pay attention to the morphological and structural changes coming from using different solutions.

Morphological and chemical characterization

In Figure 3.4 it is depicted the profilometer graph of both samples using the same condition and changing only the solution (0% and 40% of EG solution). It is clear that the outcome of the 40% electrolye showed a higher sample homogeneity growth and a smaller number of defects throughout the samples than the ones prepared without EG (0% EG). It was also optically clear that there was an improvement in the thin film adhesion when using the 40%EG solution.

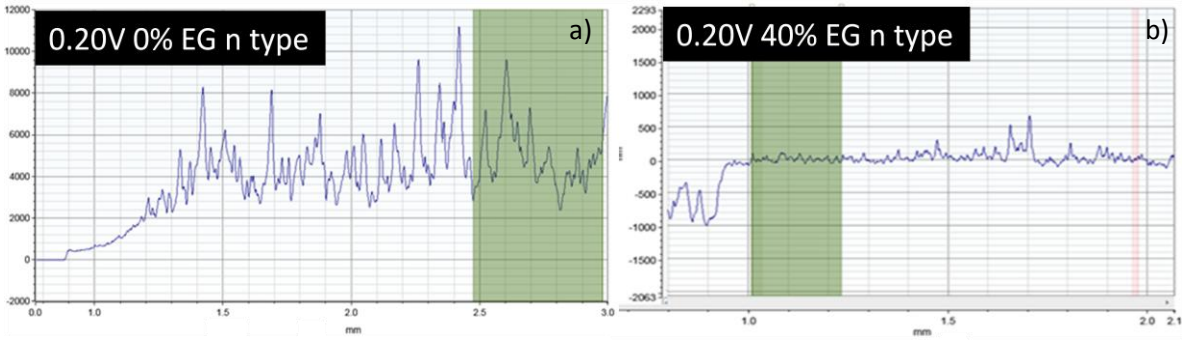

Figure 3.4. Profilometer results on a (a) 0.20 V sample made in the 0% EG n type and (b) 0.20 V sample made in the 40% EG n type electrolyte.

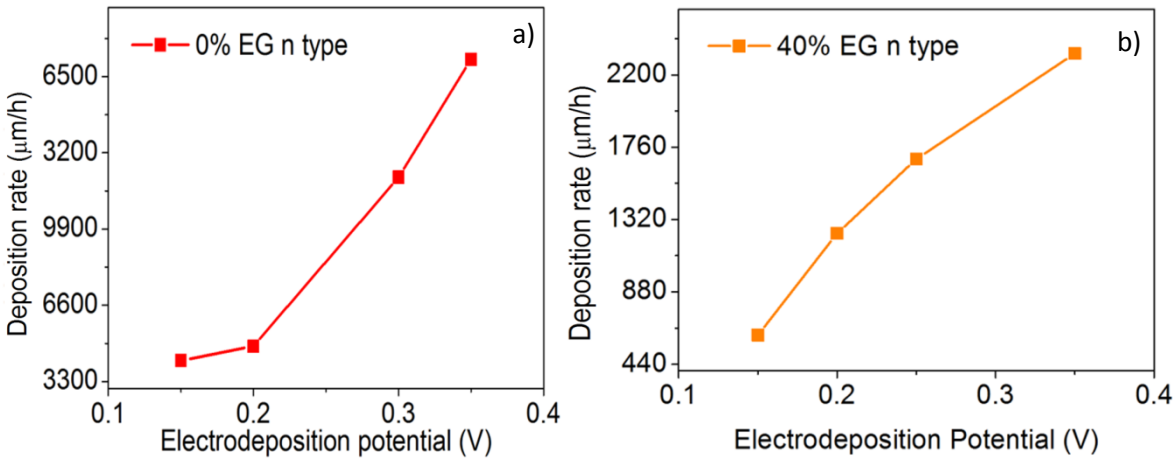

Figure 3.5. Thickness measurement results of samples deposited at several electrodeposition potentials with the same duration using (a) 0% EG n type electrolyte and (b) 40% EG n type electrolyte.

From the same Figure 3.4, it is patent that sample with 40% presents lower roughness probably connected to lower deposition rate as well as the assisted growth given by the presence of the EG [40]. As is visible in Figure 3.5 there is indeed an overall reduction in the thickness when trading from the 0% EG solution to the 40% EG (10 times lower) for the same time. This might be connected to the lower concentration of the Te and Bi ions on the overall solution, which inhibits the speed of the process, connected with 40% of the total volume being substituted with EG. Concerning the dependence of thickness with applied potential during 60 minutes [Figure 3.5], it can be observed a linear dependence which allow a better control of the thickness of thin films.

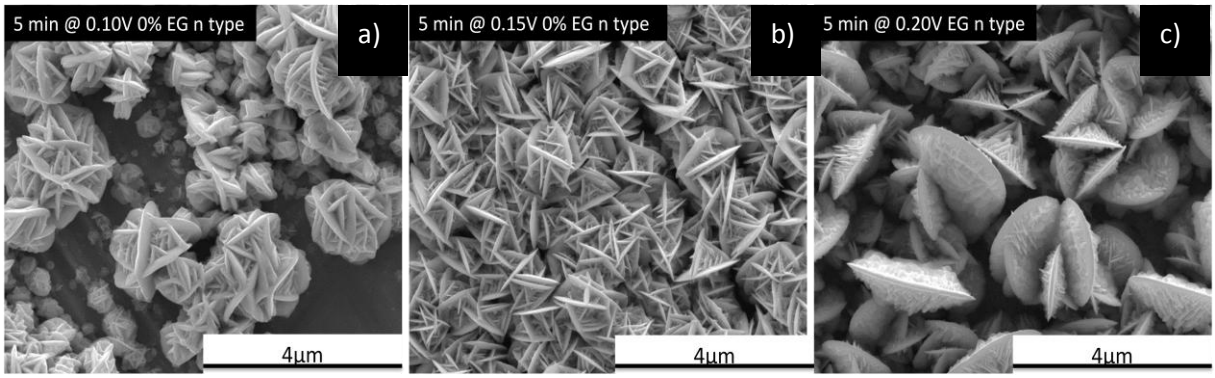

Figure 3.6. SEM results of the samples deposited using the 0%EG n type electrolyte for 5 minutes at the potential of (a) 0.10 V, (b) 0.15 V and (c) 0.20 V.

In Figure 3.6 it is depicted the SEM images for the samples prepared with 0% EG for different applied potential. It is patent that the sample by electrodeposition forms a complex cluster-like structure different from the homogeneous deposition usually obtained by other physical deposition techniques. Furthermore, there is a clear morphological sample change when the applied potential is increased showing that depending on the deposition potential, the growth process can be distinct.

The images obtained by SEM for the samples deposited at different applied potential using 40% EG are shown in Figure 3.7. Similar to the 0% EG, a clearly dependence of the morphology with applied potential is observed. Nevertheless, by comparing the samples with same applied potential for different % of EG, Figure 3.6 (b) and Figure 3.7 (a) for example, it is possible to notice that there is a significant difference in the grain size between both samples while remaining with the identical morphology. It is also possible to notice that these grains have several discontinuities which explain the high roughness presented in Figure 3.4. Furthermore, it is visible what seems like a gradual transformation in morphology between the 3 potentials presented in Figure 3.6, where the 0.15 V sample seems to be the middle step between the morphology visible in the 0.10 V and the 0.20 V samples, which would indicate a higher effect of the applied potential on thin film properties. The 0.15 V sample also showed a very good homogeneity in grain size throughout the entire sample surface without the appearance of major clusters, which showed a different tendency than the one observed on the majority of the 0% EG n type depositions. From Figure 3.7 (b) to (d) it is possible to observe what appears to be a very similar morphology between all the samples and potentials but with different cluster sizes. This indicates a similar growth tendency at these conditions which is quite different from the 0%EG counterpart. It is also due to this smaller grain size and more homogeneous

growth that there is a reduction in sample roughness when using this kind of solution. The last sample [Figure 3.7 e)] seems to show a much more dendritic growth which might indicate a different morphology for higher potentials.

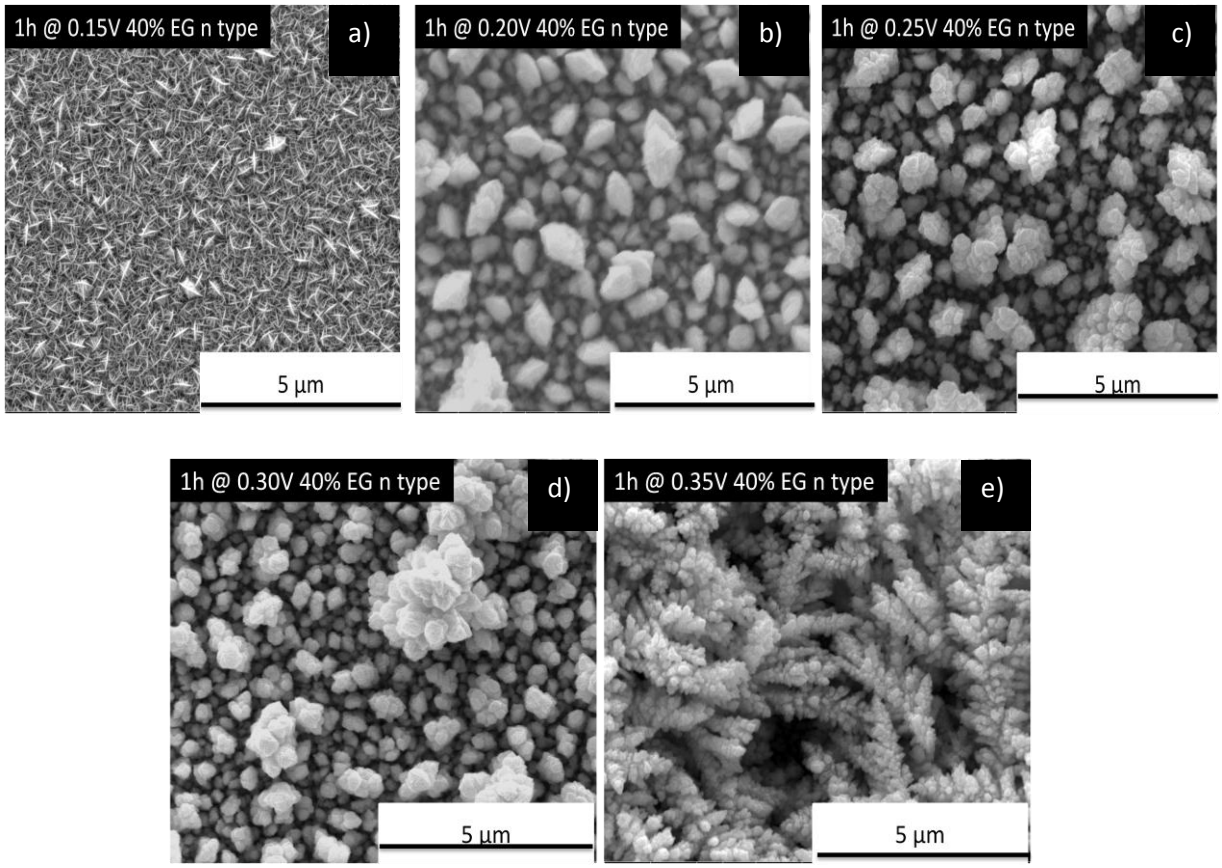

Figure 3.7. SEM results of the samples deposited using the 40%EG electrolyte for 1h at the potential of (a) 0.15 V, (b) 0.20 V, (c) 0.25 V, (d) 0.30 V and (e) 0.35 V.

Another important advantage of the electrodeposition method is the ability to control the stoichiometry of the samples which have already been found to strongly affect the thermoelectric characteristics of the samples, such as higher Seebeck coefficient near perfect stoichiometry [40]. In Figure 3.8 it is shown the effects of the electrodeposition potential on the stoichiometry of the resulting samples for 0%EG and 40%EG obtained by EDS. When comparing the obtained results it is noticeable that this variation is stronger over the 0% EG samples than it is in the 40% EG counterparts. The major variation of Bi/Te ratio is observed between 0.15 V and 0.5 V samples where there seems to be an almost linear growth in Te concentration, which stabilizes from that point forward. For the 40% EG samples the Bi:Te ratio remains almost constant (within the resolution of the EDS) but much closer to perfect Bi_2Te_3 which is a desired characteristic.

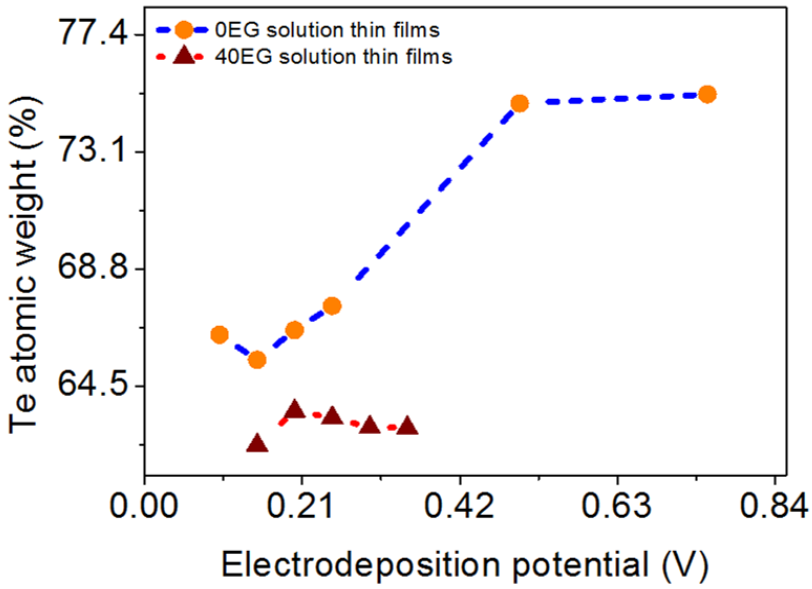

Figure 3.8. Comparison of the effect of the electrodeposition potential in the stoichiometry of the samples using 0%EG and 40% EG n type electrolytes.

Structural characterization

The XRD measurements at room temperature for the samples prepared with 0%EG and 40%EG are presented in Figure 3.9 a) and b) respectively. For the lowest applied potential (0.10 V), it is possible to notice that there is a strong tendency to have a preferential growth in the <1 1 0> direction with a minor reflexion in the <1 0 10> direction. Increasing the applied potential, it is observed that new preferential direction appears, the <0 1 5> direction followed by the presence of other reflection changing from one almost single crystal to a polycrystalline structure for 0.20 and 0.25 V. Amorphization of the samples continues to accentuate until they present very minor peaks. This phenomena probably is related with the deposition rate since higher potentials lead to higher deposition rate and since the substrate is at room temperature, for fast deposition rate, the atoms diffusion is smaller and thus leading to amorphous samples.

We remark that in Figure 3.9 (b) it is immediately clear the much smaller thickness of the thin films with 40% EG due to a strong appearance of the Pt peak followed by the clear growth in thin film thickness with applied potential. This is proved by the reduction of the Pt <1 1 1> peak, which is the strongest peak present in the 0.15 V direction sample, diminishing quickly with the growth of the deposition potential and thus the increase of Bi_2Te_3 thin film thickness. In these samples we see again a strong appearance of the <1 1 0> peak at the 0.15 V potential but there is the appearance, starting already at this potential, of the <0 1 5> peak. Not only that, but the samples do not turn as amorphous as in the previous case, since there seems to be a transition in the preferential growth direction from <1 1 0> to <0 1 5> with the applied potential. There is also the appearance of a new peak, along the <0 1 8> direction, mainly in the 0.25 V sample, which was only present in this sample case.

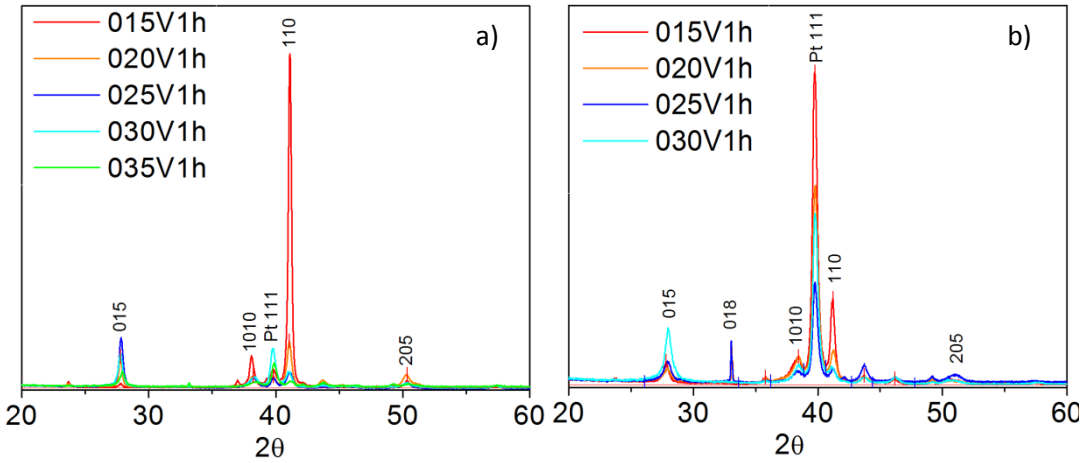

Figure 3.9. XRD results of the samples electrodeposited using the (a) 0% EG n type and (b) 40% EG n type electrolytes.

Through a refinement of Le bail [63] for all spectra the lattice parameters and the volume of different samples were extracted in the 0% EG samples. From Figure 3.10 it is clear that the **a** parameter remains constant until 0.20 V and above this potential it linearly increases, whereas the **c** parameter increases monotonously with applied potential. The volume of the unit cell was found to exhibit a similar behaviour than the a parameter [Figure 3.10(c)], which is in accordance with the EDS results [Figure 3.8] since the radius of Te ion (207 pm) is bigger than the Bi ion (117 pm) which lead to higher unit cell thus explaining the structural and chemical results.

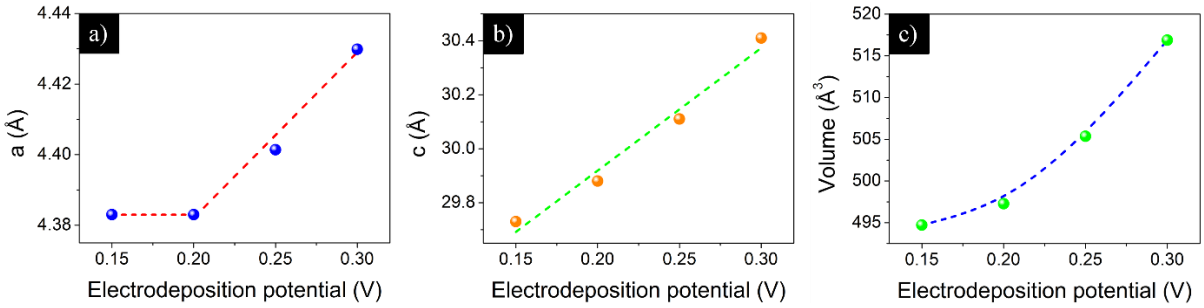

Figure 3.10. Cell parameter variations with applied potential (a) for the a direction, (b) c direction and (c) total volume.

3.2.3 P type electrolytes results

After showing the ability of controlling the deposition rate, chemical stoichiometry, crystallinity and morphology in n type samples, for the electrodeposition technique to be relevant to the industrial world on the fabrication of micro/nanodevices it should also cover the synthesis of p-type Bi_2Te_3 thin films which is being investigated in this section.

Morphological and chemical characterization

Similarly to the n-type samples, two kind of electrolytes were used 0% EG and a 40%EG for p-type solution taking into account the above mentioned results. The approach to create this semiconductor kind was based on previous works that showed that a higher amount of Bi over the perfect stoichiometry values translates in this kind of semiconductor [64]. Using profilometer technique, the

thickness/roughness was studied and the results are presented in Figure 3.11. For the samples prepared with 0% EG, very significant roughness is observed when compared with 40% EG. This results are in accordance with the obtained results for n-type again showing that smaller deposition rate leads to lower thin film roughness probably preventing an island growth more characteristic of higher potentials.

Concerning the deposition rate, Figure 3.12 shows an opposite applied potential dependence behaviour when compared with n-type materials, i.e. a decrease of the deposition rate with applied potential. This decrease is almost linear between 0.15 and 0.25 V after which it remains in an average value of ~1600 nm. The observed decrease in the deposition rate is probably connected to a strong peeling of the thin film when it is removed from the solution. In the cases where this growth is present, it can be explained by a continuous increase in dendrites size until it peels off the substrate, meaning that it seems that at higher potentials these thin films cannot be deposited without any kind of support to their structure.

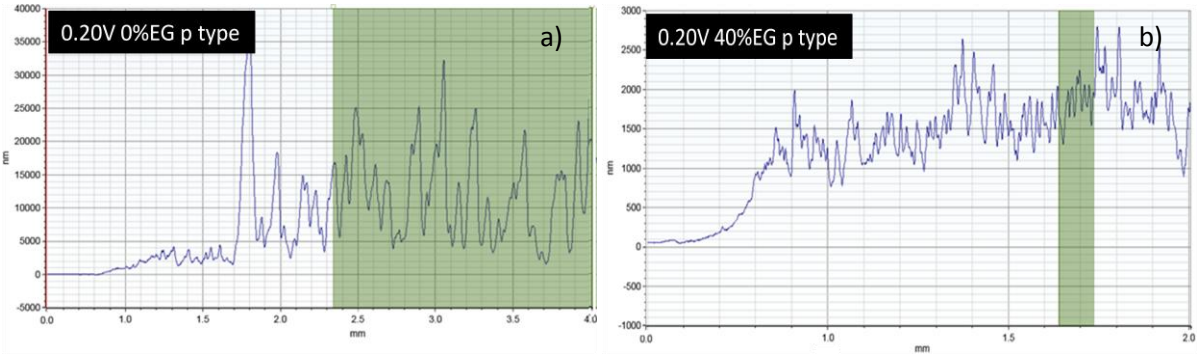

Figure 3.11. Profilometer results on a (a) 0.20 V sample made in the 0% EG p type and (b) 0.20 V sample made in the 40% EG p type electrolyte.

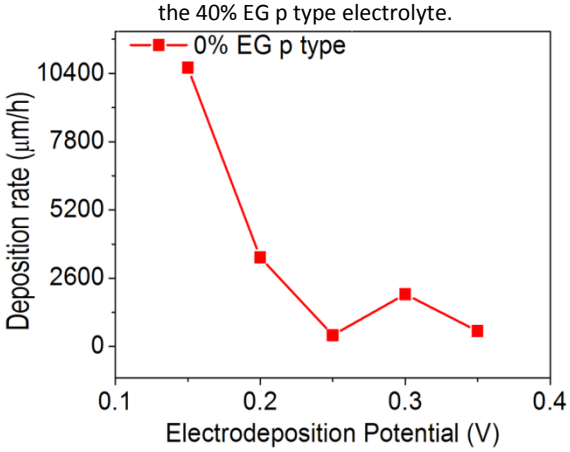

Figure 3.12. Thickness measurement results of samples deposited at several electrodeposition potentials with the same duration using 0% EG p type electrolyte.

Concerning the thin film morphological growth for the sample deposited using the 0% EG electrolyte with respect to the electrodeposition potential, it can be seen that it strongly influences the thin film's morphology with applied potential [Figure 3.13]. The morphologies observed are different from the n-type. The samples prepared with 0.15 V show a good constant growth, while the 0.20 V samples

already show significant variations in grain size. As is visible in Figure 3.13 there is a more dendritic growth present at this potential than at 0.15 V. This occurs even more strongly at 0.25 V existing an increase of this kind of growth on all the following electrodeposition potentials.

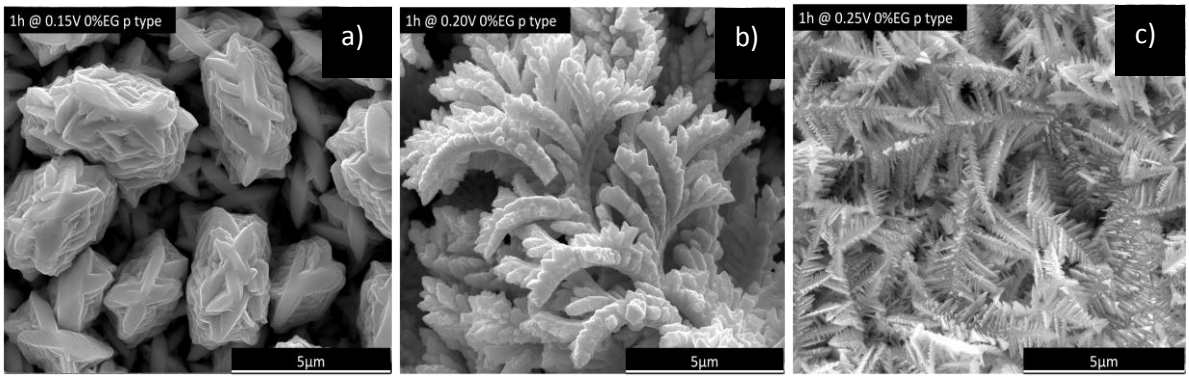

Figure 3.13. SEM images of the 0%EG p-type electrolyte samples electrodeposited at (a) 0.15 V, (b) 0.20 V and (c) 0.25 V.

The growth pattern for 40% EG samples shows again a change of the morphology with the applied potential changing from spines type structure (low potential) to a sheet-like structure (high potential) similar to previous observed in n-type (see Figure 3.14) showing that applied potential is a good parameter to control the morphology of the thermoelectric material. Comparing the samples electrodeposited at the same potentials but with different EG content, Figure 3.14 a) and Figure 3.13 a), smaller grains and less discontinuities are observed for the samples prepared with higher content of EG.

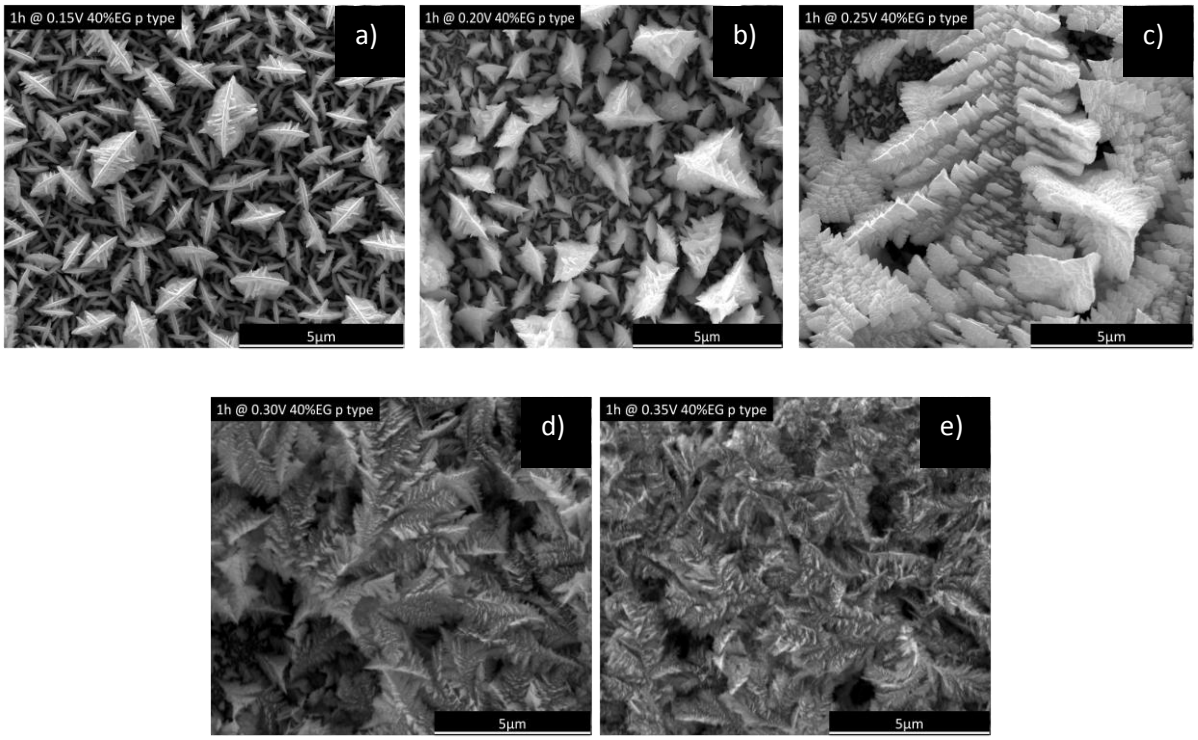

Figure 3.14. SEM results of the 40%EG electrolyte deposited for 1h at the potential of (a) 0.15 V, (b) 0.20 V, (c) 0.25 V, (d) 0.30 V and (e) 0.35 V.

Figure 3.15 shows some of the possible variations found in the thin film, which also help to explain some of the stronger variations in its thickness. These appeared only on low potential samples, mainly due to the fact that the higher potential samples had many discontinuities, which made it hard to discern any clear defects on the sample which could not be seen as normal growth patterns. An interesting information that was given with these variations, visible in Figure 3.15 (a), is that the Pt layer is not completely homogeneous, which could partly explain possible deviations on thin film growth patterns. This is the case since at the centre of this pattern it is possible to see a protruding piece of Pt. These defects are sparse throughout the sample and also allow to see that there seems to be a very good filling of the lower layers of the thin film, at these potentials, which will prove invaluable in future measurements of the Seebeck coefficient, a kind of measurement that requires a good covering of the conductive layer.

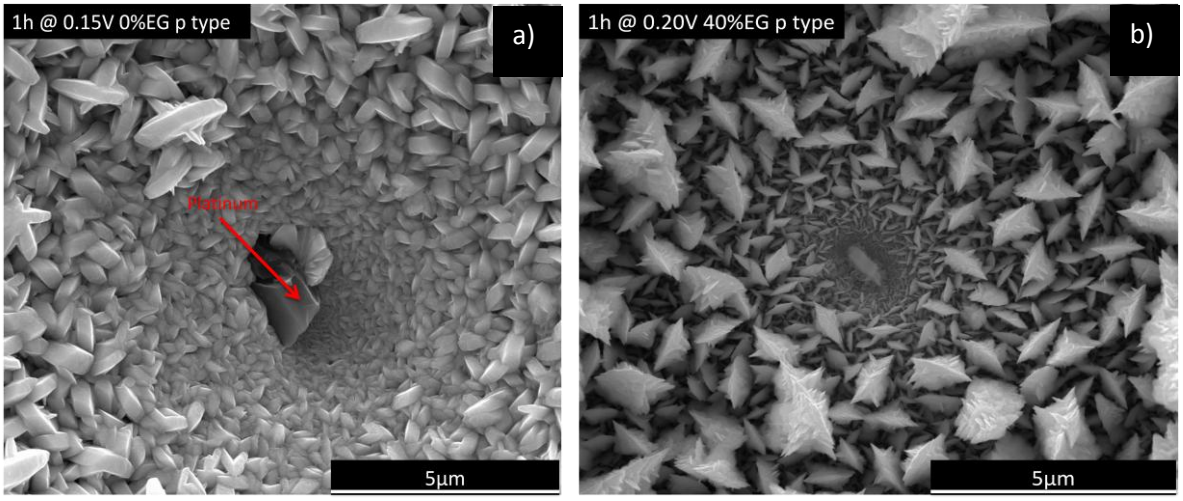

Figure 3.15. SEM images of growth abnormalities in the (a) 0.15 V 0%EG and (b) 0.20 V 40%EG samples.

A key parameter for high efficient thermoelectric materials is the stoichiometry namely to guarantee that the 60% atomic weight of Te is not passed to create the possibility to have a p type sample. Figure 3.16 shows the relation studied between the applied potential and the Te atomic weight % of both 0% and 40% EG p type solutions. From Figure 3.16 it is clearly observed that there is a strong relation between % of EG and the chemical stoichiometry. Using the 0% EG electrolyte, a linear relation is obtained between the Te amount and the applied potential. This indicates that the potential affects quite strongly our stoichiometry in this electrolyte. In the case of the 40% EG solution, there is no apparent relation between the electrodeposition potential and the stoichiometry, seen in the form of a nonsensical line between samples [Figure 3.16]. This knowledge can be taken advantage off by fine tuning the concentration of Bi or Te ions in the future solutions to reach a certain desired Te atomic weight % content [64].

These variations are similar to the ones seen before in the n type solutions, which indicate that this might be characteristic to the presence of the EG in the electrolyte.

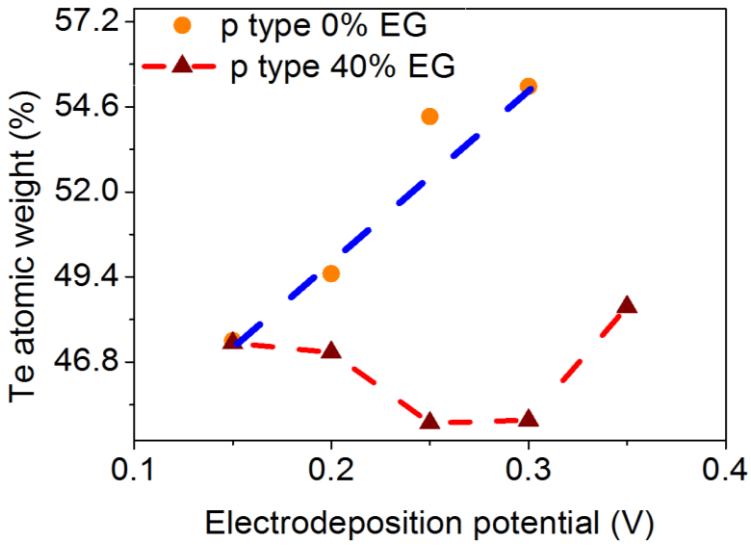

Figure 3.16. Effect of the electrodeposition potential on the sample's stoichiometry using the 0% EG and 40% EG p-type solutions.

Structural characterization

The XRD measurements, seen in Figure 3.17 (a), show a pattern quite similar to the one found in the n type study [Figure 3.9 (a)], following the tendency of a growth along the <1 1 0> direction at low applied potentials, which is highly crystalline with a minor peak along the <1 0 10> direction. As was observed, there is an amorphization with the increase of the applied potential accompanied by the growth of a new peak along the <0 1 5> direction, which also diminishes quickly with the applied potential. The increase of the Pt peak's intensity in the 0.3 V sample might be connected to higher discontinuities in the thin film, which are more likely to expose the Pt layer. It is also important to notice that, both in Figure 3.17 (a) and Figure 3.9 (a), the 0.20 V sample shows a small peak along the <2 0 5> direction, which is almost absent on all other samples.

In the case of the 40% EG samples, seen in Figure 3.17 (b), the same crystalline growth is visible at 0.15 V with a preferential growth along the <1 1 0> and <1 0 10> directions. The amorphization process is also highly present in these samples but, while it kept growing with the applied potential on the 0%EG samples, this is no more the case. The new preferential growth direction, <0 1 5>, does not reduce in peak size when increasing the applied potential, which indicates that these samples show a stable preferential growth along this direction even at higher deposition potentials. It is also important to note the presence of a strong Pt peak in all samples, except at the 0.15 V, which indicates a smaller thin film thickness. This peak is not as visible in the 0.15 V sample due to high covering of the Pt surface due to a much more homogeneous growth.

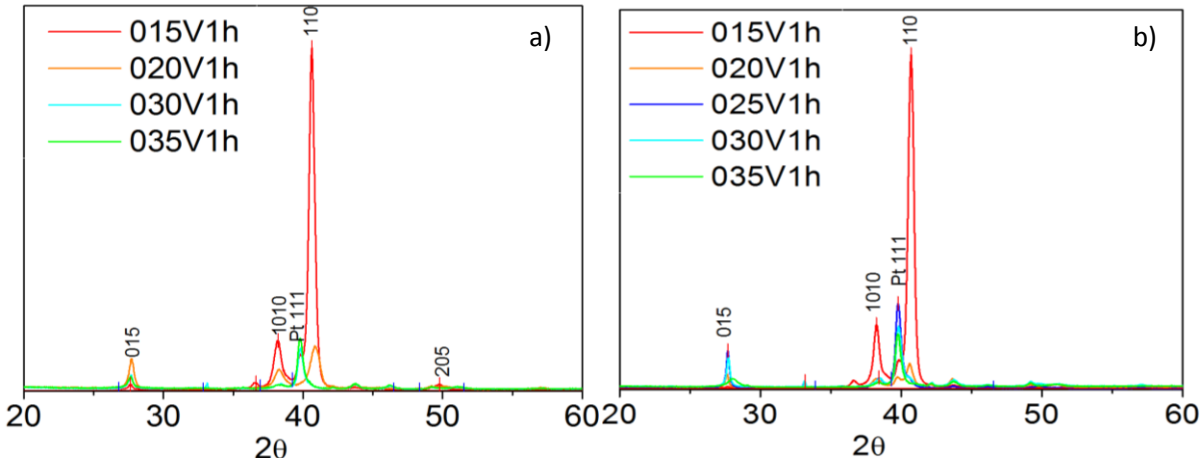

Figure 3.17. XRD results of the (a) 0% EG p type and (b) 40% EG p type electrolyte samples.

3.2.4 Seebeck coefficient and electrical conductivity measurements

By using the developed Seebeck measurement apparatus in Figure 2.6, a Bi_2Te_3 thin film electrodeposited on a Cu stripe substrate in the n-type 0%EG solution was measured. However, as is visible by comparing Figure 2.7 (b) with Figure 3.18, the sample measurement and specially the slope, are too similar to that of the Cu stripe, giving the same Seebeck coefficient values, which indicates that what is actually being measured is not the electrodeposited material but the Cu underneath it. Several reasons might explain this effect, such as the sample's porosity, which may allow for the silver paint (used to connect the Pt wires to the sample) to short circuit with the copper making it impossible to study the thin film. Another possible explanation is the small thickness of the sample [65] that may allow for the current to reach the copper stripe thus creating again a short circuit. The obtained results are a obvious evidence that the method of the Seebeck measurements for thin film should be improved. To solve this issue, one of the approaches is depositing a significantly thicker film to make sure the conductive substrate is never reached or that the current is able to escape through it. Another possible solution is moving the thin film unto a non-conductive surface. This approach has several different steps that need to be applied to remove the electrodeposited thin film from its contact and place it on top of a non-conductive substrate [66]. Otherwise there is a high possibility that most of the current will pass through the metallic substrate underneath, making it impossible to properly measure the thin film's Seebeck coefficient.

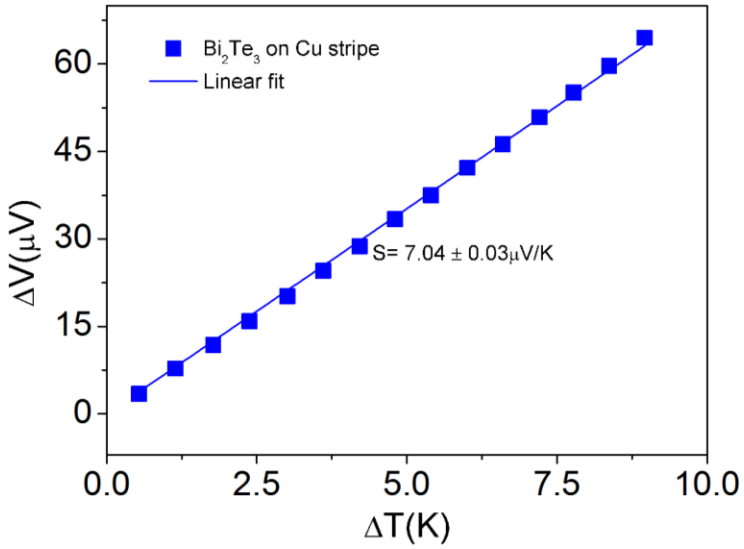

Figure 3.18. Seebeck coefficient measurement of a 0% EG sample on Cu stripe deposited at 0.25 V.

In Table 1 are reported the results of electrical resistivity at room temperature for 0%EG thin films. The majority of the samples present resistivities of ~ 15 mΩ cm with the exception of the sample deposited at 0.2 V, which presents a resistivity with one order of magnitude higher (106.9 mΩ cm). Nevertheless, the obtained results for the majority of the samples are ten times higher than the obtained in other reports which is of the order of 1 mΩ cm [67]. This might be connected to measurement induced errors, such as wires-to-sample contact resistivity or sample's inhomogeneities which diminish the reliability of this measurement process. A clear relation between the thickness/deposition rate and electrical resistivity is observed, meaning that probably during the electrodeposition process defects are being formed. The obtained results may arise from the anomalous microstructure as mentioned above, namely on the formation of aggregates with exotic shapes during the material forming clusters. Since the electrical resistivity is a short range effect, there is a possibility that the electrons passing between clusters suffer higher scattering leading to higher electrical resistivity. Additionally, the rate of deposition can play an important role since fast growing rate can lead to higher defects. Contrary to the atomic structure which varied largely with the applied potential, the crystallite size, calculated using the equation (2.4) does not change significantly with deposition potential leading to a mean value of ~15 nm.

Potential (V)	Thickness (μm)	Crystallite size (nm)	Resistivity (mΩ cm)
0.15	1.79	14.5	11.2
0.20	6.48	13.1	106.9
0.25	4.70	15.3	21.2
0.30	3.30	17.2	17.0

Table 1. Electrodeposition potential effect on several thin films properties.

3.3 Conclusion

With the aim to study and develop the best parameters for the creation of microdevices based on the electrodeposited p-type and n-type pillars, the designing and optimization of thin films of Bi_2Te_3 has been conducted. All four electrolytes used have shown different properties and advantages over each other. The 0% EG solutions show much higher deposition rates and higher variations on the sample's stoichiometry, which might allow to pick the best one to obtain the best thermoelectric properties. The 40% EG electrolytes show a significant diminish in thin film rate of deposition, which gave rise to a much more homogeneous growth of the resulting samples with different morphological results. It is also possible to notice that low potentials, such as 0.15 V, show an almost single crystalline growth along the <1 1 0> direction in all electrolytes. This is a quite important result due to the possibility to reach the higher values for electrical conductivity necessary. Furthermore, EG allows to control the thin film roughness, which helps to create stable pillars with higher adhesion. A strong study has been conducted in the optimization of the stoichiometry of the samples, aiming the perfect Te atomic weight for the appearance of both p-type and n-type Bi_2Te_3. It was also shown that the 40% EG solutions have a much more stable Te stoichiometry simply by fine tuning the concentration of Bi and Te ions in any future solutions. Seebeck measurements have shown that the apparatus is fully functional with a constant error and, even though the sample measured did not show the thin film Seebeck coefficient but the Cu under it, which indicate that improvements still need to be made. The electrical resistivity results presented are also higher than the ones expected showing that optimized control of the nanostructures should be address. Therefore, future work on the annealing of these samples and other improvements are still needed, which will highly improve these results.

Chapter 4
Electrodeposition of Bi_2Te_3 nanowire arrays

4.1 Introduction

The predictions that 1D structures will become the most efficient thermoelectrics in the future has spurred a strong interest in developing and creating Bi_2Te_3 nanowires (NWs). Due to the low cost, easy scalability and fast deposition rates, template-filling electrodeposition techniques were chosen for the NWs growth. PAA was picked as the template for a number of reasons such as the possibility of reaching very small pore diameters (minimum ~6 nm) [68], easy reproducibility and very high level of organization of the porous array. Some other very important characteristics of PAA templates are a very high pore density, high stability, resistance to high temperatures and resistance to organic solvents.

The main objective behind the work developed in these NW structures was to fully control the growth process, such as the distinct phases present in the NWs, the quality of the pore filling, the uniformity of the NWs length, and the deposition of a good effective area of Bi_2Te_3 NWs. Another important characteristic was the control over the stoichiometry of the resulting samples. Small variations around the perfect stoichiometry are known to strongly influence this material's thermoelectric properties and even its growth pattern inside the pores [34]. In addition, it is also very important to understand the effects of the electrodeposition potential on the sample's quality and properties, aiming to achieve the best deposition parameters for the application of these nanostructures in future devices. The variation in the NWs length is influenced by several factors, such as the membrane's behaviour after long deposition times, and small defects that might appear during the deposition process. The analysis of the deposition current transients also allows one to better understand the NWs growth inside the porous membrane. Finally, the XRD results illustrated the presence of different crystalline structures depending on the electrodeposition potential used, which is very important for future applications, as the cristallinity and direction of growth of this material highly influences its thermoelectric properties. The solution used for this process was the 0% EG n type solution.

4.2 Results and discussion

4.2.1 Electrodeposition current transients

The careful analysis of the electrodeposition current transients already allows one to study the NWs deposition rates and overall growth characteristic without the need of using expensive equipment such as SEM or XRD. As shown in Figure 4.1(a), the typical current transient curve of NWs being deposited in PAA templates at a constant potential starts with an abrupt reduction in current. Similar to the thin films this happens due the creation of the first layers of our semiconductor material, which has a much higher resistivity than the Au contact layer at the bottom. The stable current thereafter can be understood as an approximately constant growth of Bi_2Te_3 NWs inside the pores throughout

the entire exposed membrane. Figure 4.1 (b) shows a comparison between the deposition current transients of NWs electrodeposited at different applied potentials. The majority of the samples present very similar electrodeposition curves, with the exception of the sample deposited at 0.75 V which, as will be shown later, has a very different stoichiometry. It is important to note that this figure is highly zoomed, as to better distinguish between the deposition curves. The much higher current obtained for the sample deposited at 0.75 V hints to the presence of a higher concentration of Te in the sample, since this element tends to have a much higher reduction rate than Bi (see 2.2.3). Overall, the deposition curves of the samples deposited at lower potentials present a much more stable current throughout the entire deposition process, while those at higher potentials present higher variations. When comparing NWs deposition in a nanoporous template with thin film deposition on a flat substrate (chapter 3), one notices that the deposition current is significantly lower in the former case. This is ascribed to the effective deposition area, which is much lower in the NWs case, as a good part of the area exposed to the electrolyte (around 70-80%) is the alumina membrane.

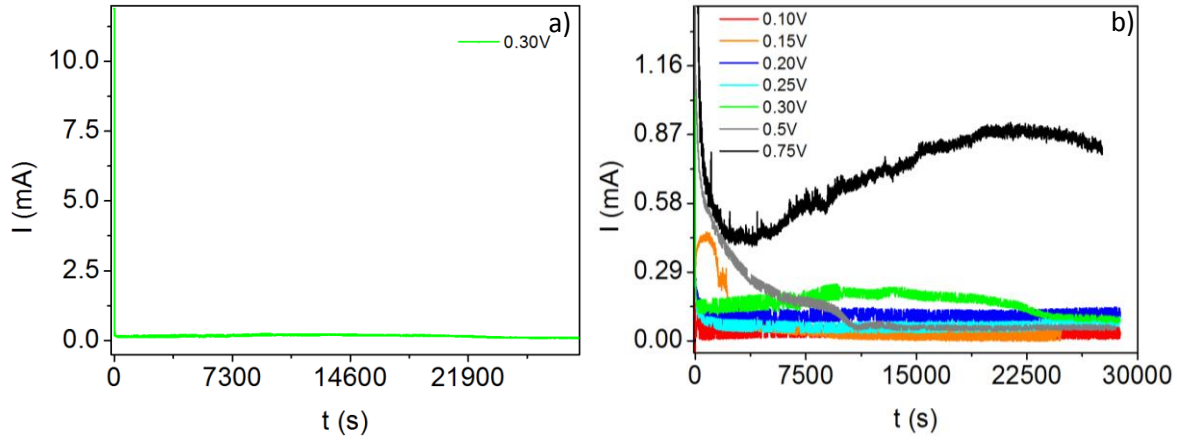

Figure 4.1. Representation of the electrodeposition current transients monitored during (a) a typical NWs deposition process at 0.3 V, and (b) the NWs deposition at different applied potentials.

4.2.2 Morphological characterization

To better understand the deposition process inside the nanopores, SEM cross-section and bottom imaging of the filled template was performed. For the bottom SEM imaging, the Au contact layer was previously removed and the sample smoothed by etching 200-300 nm of its surface using ion-beam milling. Figure 4.2 shows cross-sectional SEM images of PAA templates filled with Bi_2Te_3 NWs deposited at different potentials for 8 h. An homogeneous pore filling is found until about half of the membrane's thickness, after which the top pores start to be simultaneously clogged with Bi_2Te_3 clusters. This may occur due to the presence of smaller pores at the template grain boundaries, which will be filled at a faster rate, reaching the upper surface sooner. These will then create small clusters at the template's surface, which will block the subsequent pore filling thus forming bigger clusters [Figure 4.2(a) and (c)] or even a continuous film [Figure 4.2(b)].

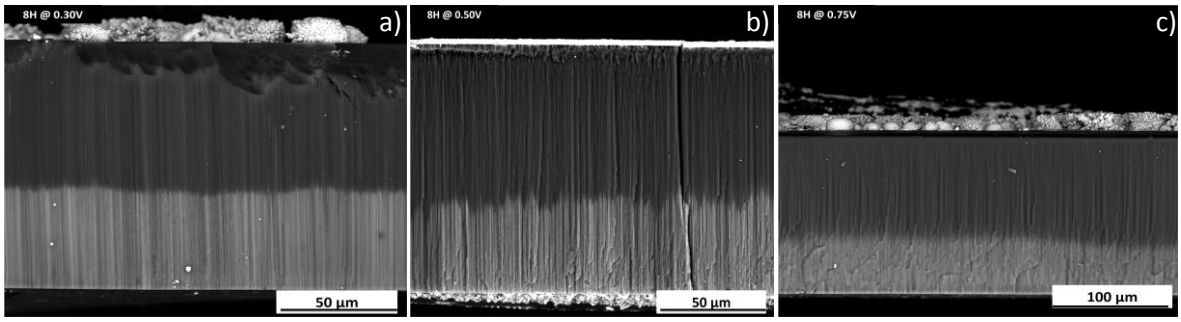

Figure 4.2. Cross section SEM views of the whole PAA with Bi_2Te_3 nanowires deposited at (a) 0.30 V, (b) 0.50 V and (c) 0.75 V for 8 h.

Another important result is found when analysing the bottom surface of the filled porous template. Figure 4.3 shows bottom SEM imaging of several samples deposited at different potentials for 30 min. The PAA structure exhibits the characteristic highly ordered hexagonal array of pores, with a pore diameter of 50-60 nm and an interpore distance of around 105 nm, evidencing the good reproducibility and control of the anodization processes. As for the pore filling, its quality was found to highly depend on the applied potential during the deposition process. Figure 4.3 (a) shows a complete and homogeneous pore filling when applying low potentials (0.15 V). However, when increasing the applied potential there is a clear decrease in the quality of this filling process, where thinner and granular-like nanowires are obtained [Figure 4.3 (b) and (c)]. At lower potentials, there is a slower rate of deposition promoting a smoother and better nucleation of the material inside the pores. By increasing the applied potential the deposition rate will also increase, impelling the growth process to occur in a more inhomogeneous way (granular-like), which can sometimes also lead to the simultaneous deposition of impurities.

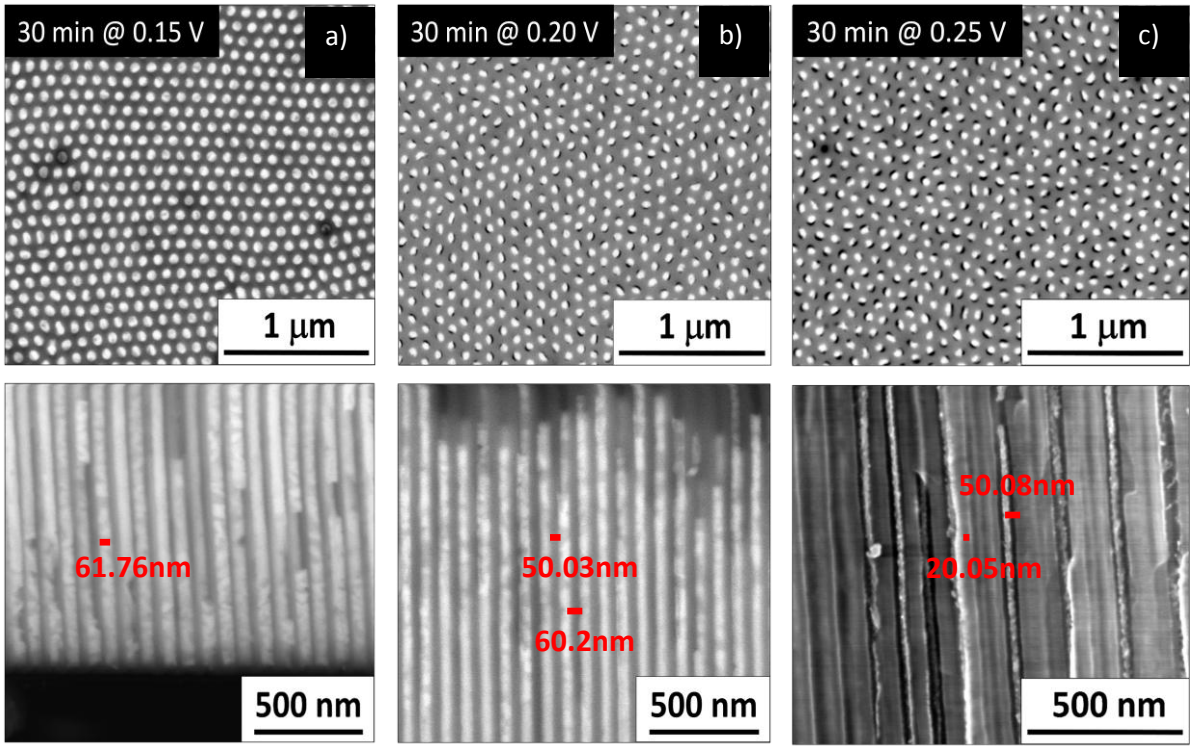

Figure 4.3. Bottom and cross section SEM views of the NWs electrodeposited at (a) 0.15 V, (b) 0.20 V and (c) 0.25 V for 30 min.

The combination of high growth rates alongside with good homogeneity of pore filling throughout the entirety PAA template are two very important factors for the future application of these structures into nanodevices. The main aim is to ensure that the maximum number of NWs, or, equivalently, the total effective area of the device, are being used. As shown by SEM imaging in Figure 4.4, the NWs' length is quite homogeneous throughout the whole template, at every applied potential, which is a very important result. It is also possible to note that the growth rate varies strongly with the applied potential [Figure 4.5], as expected, increasing significantly at higher potentials (> 0.5 V). The lower rates obtained are around 2.71 and 5.15 μm/h at 0.15 and 0.20 V, respectively, while the higher rates can reach values of around 67.32 and 44.4 μm/h at 0.5 and 0.75 V, respectively. However, when applying higher potentials these values quickly drop at the latter stages of the deposition, mainly due to the appearance of clusters on top of the template, as previously shown in Figure 4.2, which will inhibit the further normal NWs' growth.

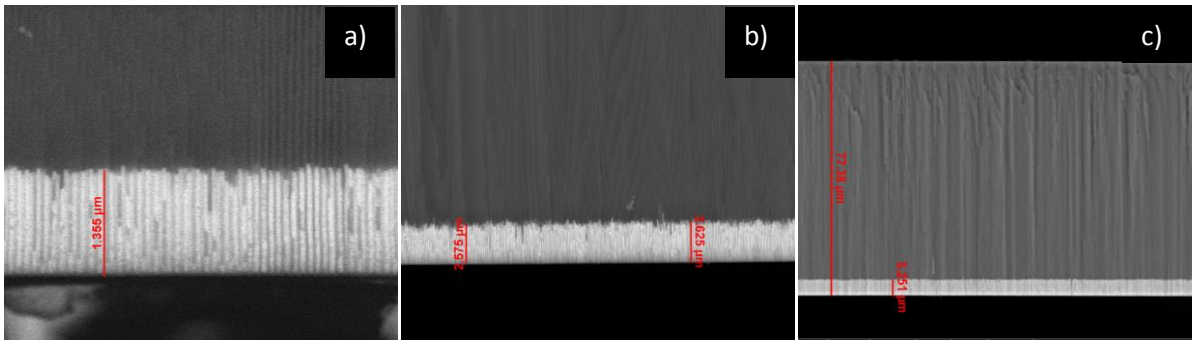

Figure 4.4. Cross section SEM views of the NWs electrodeposited at (a) 0.15 V, (b) 0.20 V and (c) 0.25 V for 30 min.

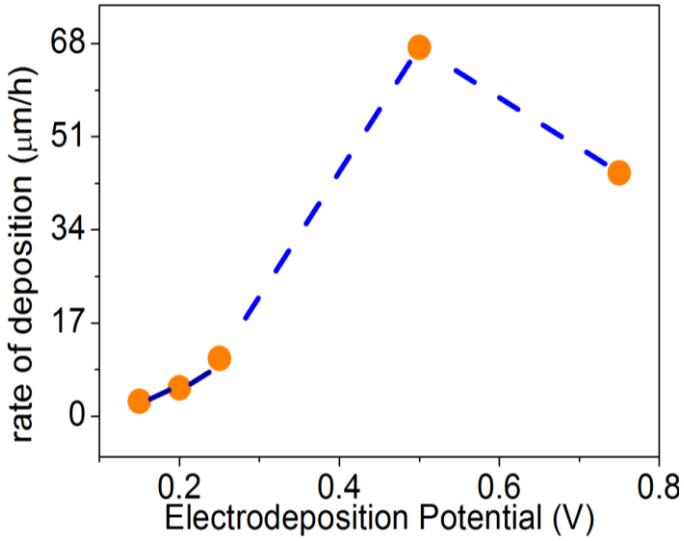

Figure 4.5. Rate of deposition based on the estimation of the NWs length from SEM cross-sectional images.

4.2.3 Stoichiometry analysis

The ability to change the semiconducting type of Bi_2Te_3 from n-type to p-type with only a variation of around 2-3% of Te [64], boosted a strong desire to accurately control the stoichiometry of the deposits. In this work, the stoichiometry of the electrodeposited NWs was studied by EDS, similar to the previous performed in thin films [Figure 3.16]. Figure 4.6 shows the variation of the Te atomic weight percentage present in the NWs, as a function of the applied deposition potential. The Te% content was found to increase linearly with the applied potential, ranging from around 60% (Bi_2Te_3) at 0.15 V to around 90% ($BiTe_9$) at 0.75 V. This behaviour gives the possibility to accurately tune the stoichiometry of the deposited NWs, by simply controlling the applied potential during the deposition process, allowing the future fabrication of segmented NWs with different compositions. In addition, the control over this stoichiometry will allow one to fabricate NWs mainly composed of Te or even control the growth of p-type and n-type Bi_2Te_3, which is very near the 60% Te concentration.

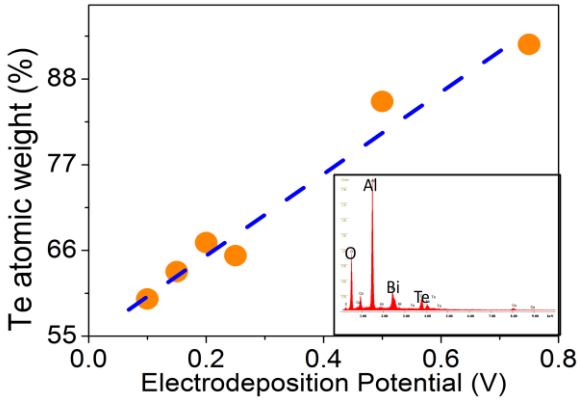

Figure 4.6. Effect of the electrodeposition potential on the nanowire's stoichiometry. Inset shows a typical EDS measurement of the nanowires in the PAA.

4.2.4 Crystallographic structure

The XRD analysis has shown that the samples crystallinity is also highly dependent on the electrodeposition potential. As represented in Figure 4.7, the NWs electrodeposited at 0.10 V exhibit a Bi_2Te_3 crystallographic structure highly textured along the <1 1 0> direction. This result has never been reported before for NWs grown by a potentiostatic deposition process but which has been shown in a pulsed electrodeposition [34]. It is also noticeable that the crystallinity of the NWs decrease significantly with the applied potential. For intermediate potentials (0.15-0.20 V) the NWs become poli-crystalline, and at high cathodic potentials (>0.3 V) amorphous structures are obtained. This is visible by the significant peak <1 1 0> intensity reduction when going from 0.10 V to 0.15 V applied potentials. In addition, at 0.15 V the NWs exhibit also a crystallographic structure along the <0 1 5> and <1 0 10> directions. The further reduction of these crystallographic peaks is then observed when increasing the applied potential, almost disappearing for samples deposited at around 0.20 V. The complete conversion into an amorphous growth occurs when further increasing the applied potential, where a complete disappearance of all peaks is observed for samples deposited at 0.30 V

and 0.75 V. This seems to be related to the higher deposition rates and poorer pore filling, which impede the formation of crystalline structures thus promoting a much higher amorphous growth inside the pores.

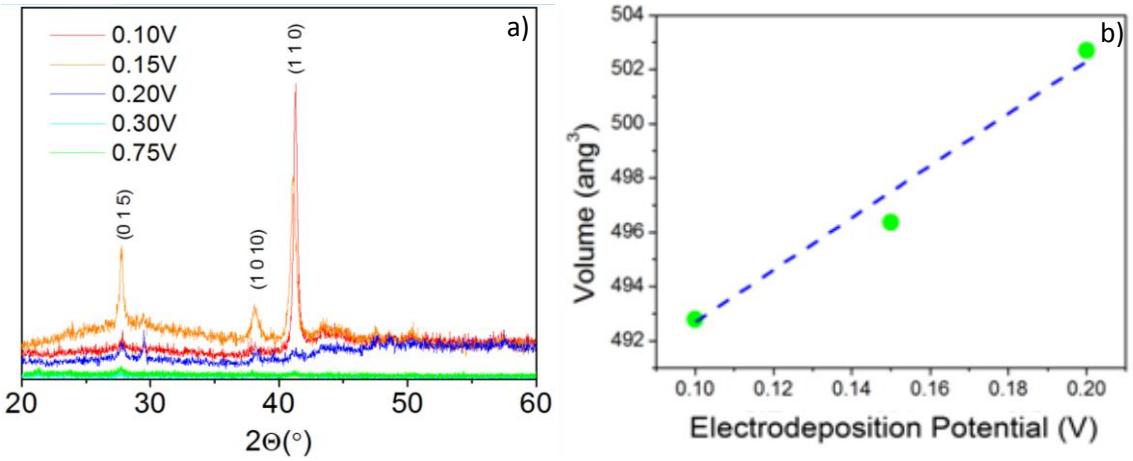

Figure 4.7. (a) XRD spectra of the nanowires electrodeposited in the PAA templates at different potentials. (b) Variation of the volume of the unit cell with the applied potential.

As described in the previous chapter, the volume of the unit cell was estimated by performing Le bail refinements in the XRD spectra of the samples deposited at lower potentials. Figure 4.6 (b) summarizes the results obtained, illustrating the influence of the applied deposition potential on the crystallographic structure of the Bi-Te deposits, where the unit cell volume is shown to increase with the applied potential. This is due to the fact that Te^{2-} ion has a bigger ionic radius (207 pm) than that of Bi^{3+} ion (117 pm), meaning that a higher concentration of Te would form a unit cell with a bigger volume.

Concerning the crystallite size (d_{XRD}), this was estimated using the Debye-Scherrer equation (2.3) for the reflection <1 1 0> The crystallite sizes obtained are summarized in Table 2. As can be seen, the crystal sizes of the samples deposited at lower potentials are similar to the radius of the NWs (around 25 nm). However, when increasing the applied potential the crystallite sizes decrease very fast, which hints again to the formation of more amorphous grown structures.

Potential (V)	Length (µm)	Crystallite size (nm)
0.10	1.	24.7
0.15	1.5	17.0
0.20	2.7	13.8
0.25	5.4	N/d

Table 2. Nanowire length and crystallite size measured at room temperature for the different applied potentials.

4.3 Conclusions

Aiming the accurate control and optimization of the growth processes of Bi_2Te_3 NW arrays, a thorough study of the effects of the electrodeposition potential in the crystallinity, stoichiometry, rate of deposition, growth patterns and pore filling process have been conducted. The analysis of the deposition current transients combined with the SEM imaging, allowed us to discern the growth process of these structures. A complete pore filling was obtained at lower potentials and a much poorer pore filling was observed at higher potentials. A deposition time limit has been established from 8 to 10 h, at room temperature, before the solution completely etches the PAA, thus destroying it. Further SEM imaging has allowed us to observe a homogeneous distribution of the NWs height throughout the membrane, which is a very important characteristic to have the maximum efficient area for future devices. The rate of deposition was found to be highly dependent on the applied potential, increasing with it, as expected. XRD and EDS measurements have allowed us to conclude that higher potentials lead to the deposition of higher concentrations of Te, having been shown that at 0.10 V the samples present an almost perfect stoichiometry, while at 0.75 V almost 90% of Te is obtained. It was also possible to observe a single crystalline growth along the <1 1 0> direction for the sample deposited at 0.10 V, which quickly turned into a poli-crystalline sample at 0.15 V and then mostly amorphous at 0.3 V. A thorough and systematic study of the electrodeposition process of Bi_2Te_3 nanowires has been conducted, all of which will in the future allow for the creation of thermoelectric nanodevices based on this principle.

Chapter 5
Fabrication of Bi_2Te_3 microgenerators prototypes

5.1 Introduction

This chapter is devoted to an initial phase on the development and creation of microgenerators prototypes using electrodeposition technique at IFIMUP-IN. Moreover, different levels of complexity and optimization were tackled, and thus two types of lithography processes have been proposed, being only one of them fabricated and used for preliminary efficiency studies. The prototype built is constituted by a simple array of pillars produced by a combination of lithography and electrodeposition processes, thus growing n-type or p-type pillars over a flexible substrate. Two different prototypes have been produced using this process, one with pillars only of the n-type and the other with pillars only of the p-type. The aim was to better understand the measurement processes and properties. A numerical simulation was also done in order to compare the theoretical results with the obtained measurements. A second process for a full fabrication of the thermoelectric generator is described showing the ability for being scalable to industrial application.

5.2 Working prototype

The ability to create both p and n-type pillars using low-cost techniques is fundamental for the successful fabrication of a microthermoelectric device. This aim spurred the development of a device based solely on a simple square array of circles with 250 μm radius and a total area of $1cm^2$ which translates in a total of 100 pillars.

Due to the simplicity of the lithographic step of this process, the main techniques used for its creation were a spinner, the direct laser writing technique, the electrodeposition process and a single thermal evaporation of Cu. The process started with a thorough cleaning of the ITO substrate in acetone, followed by ethanol and finally deionised water in ultrasounds bath, 10 minutes each step. Then, in order to create the pattern, a S1818 photoresist was coated unto the cleaned substrates with an initial speed of 500 rpm for 10 seconds followed by 4500 rpm for 30 seconds. The choice of photoresist was based on the preference to use a fully controlled and well known process, which was the case for this polymer. After this was done, a soft bake at 100°C for 1 minute was conducted. At the end, the estimated thickness was of about 2-3 μm. The drawing of the pattern was done directly on the substrates, taking about 50 minutes to complete. After, the written part was lift-off using a the revealing solution of this photoresist.

Concerning the filling of the microhole, the electrodepositions were performed for 1 h using the 0% EG n-type and 0% EG p-type electrolytes to grow the n-type and p-type semiconductor legs, respectively. Due to the higher resistivity of the ITO a 0.25 V potential was applied to completely fill the 2-3 μm height of the photoresist. This potential was chosen considering the results obtained in the previous chapters (Chapter 3 and Chapter 4). To seal the microdevice, after the completion of the

electrodeposition process the samples were submitted to a thermal evaporation of Cu unto the revealed top of the pillars. The Cu top layer was about 75 nm thick and serves as an electrical contact to close the circuit. The resulting devices can be seen in Figure 5.1.

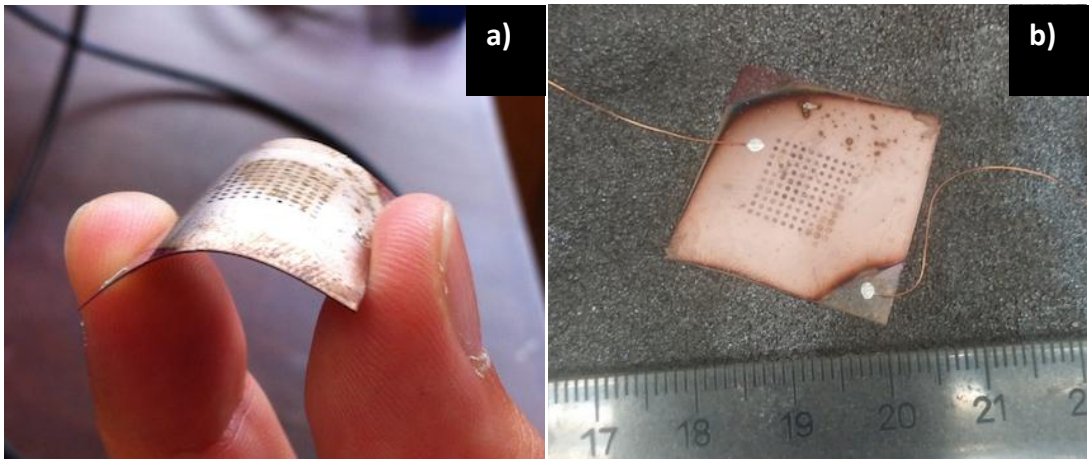

Figure 5.1. Photographic proof of the (a) flexibility and (b) small size of the devices developed.

These devices were then, as shown before [Figure 2.9], wedged between two Peltier devices to create a controlled temperature gradient and to measure the output potential with the varying temperature. Figure 5.2 presents the thermoelectric potential generated as a function of temperature gradient between top and down part of the microdevice for the n-type and p-type microdevices. A linear behaviour is observed in both cases as expected from the relation between Seebeck effect and the temperature gradient. From the potential signal one can confirm the nature of the semicondutores produced. A positive (negative) slope is obtained in the microdevice filled with a p-type (n-type) semiconductor, showing that the Seebeck coefficient arises from the hole (electron) carriers. Nevertheless, the obtained slope values, 17.79 and -13.35 μV/K for the p-type and n-type samples, respectively, are far from the expected one, which is of around 200 μV/K for bulk [18]. It is noteworthy that this allowed to confirm that the pillars were correctly filled and that the device, even though quite simple, can already be used to generate small amounts of potential.

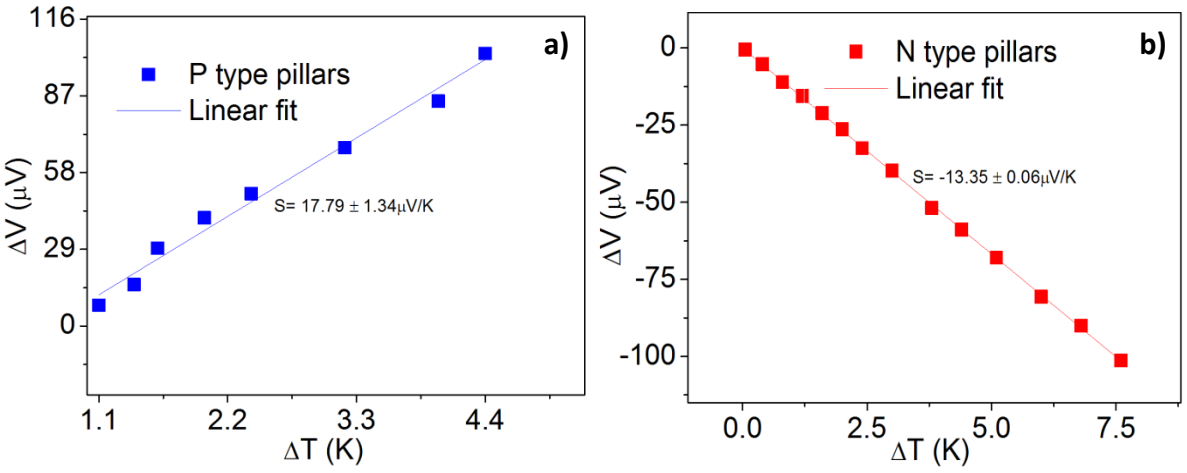

Figure 5.2. Device potential measurements of (a) p type pillars and (b) n type pillars on flexible substrate.

In the ambit of a PEEC ("Programa de Estágios Extra-Curricular") which was supported during this work, a simulation in COMSOL of six pillars of an n-type Bi_2Te_3 material was done in parallel to the development of this prototype, in order to compare the obtained results with theoretical ones.

The simulation was done with a ΔT of 3°C having shown a much higher electric potential (-600μV) which is connected to the use of the theoretical Seebeck coefficient of this material [Figure 5.3 a)] [61]. A simulation of the current density of these materials is also shown [Figure 5.3 b)], to give an idea of the current passing through the system, which is an important parameter in the estimation of the device's power output. Experimental measurement of this value still has to be made.

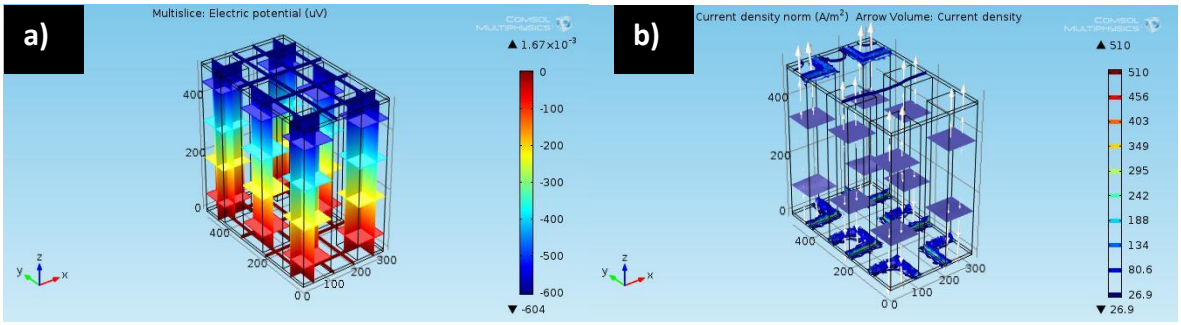

Figure 5.3. COMSOL simulation of a six pillar system of Bi_2Te_3 showing the (a) electrical potential and (b) current density with a ΔT of 3 °C.

5.3 Design of functional thermoelectric microdevice concept

With the aim to create a highly efficient microgenerator, the concept of a fully produced device based solely on lithography methods and electrodeposition has been engineered, planned and designed, only missing the realization of the prototype. From the obtaining planning, the techniques required for this process are: direct laser writing for the creation of the lithography mask or for direct printing unto a previously prepared substrate; the correct use of photoresists to create the desired patterns on the target of the writing, this encloses spinner, baking and lift-off processes; a process for the deposition of the conductive layer, either sputtering, electron beam deposition or thermal evaporation, depending on the conductor used; and finally the proper and controlled electrodeposition process developed in this thesis.

An important aspect for the development of an efficient thermoelectric microdevice is the photoresist used, which should be SU-8 [69] negative photoresist, mainly due to its physical properties such as low thermal conductivity (0.3 W/mK), high thickness and high resistivity (~10^{16} Ωcm). The electrical contacts to be used have yet to be established, although both Au and Pt have shown good results and stability as previous observed in 3.2.1. The wish to use less expensive conductors still exists and preliminary studies in ITO and Cu still continue. Concerning the substrate, it will vary depending on the desired characteristics of the sample. If the creation of a flexible sample is necessary, ITO will possibly be the main substrate. If the sample has a more rigid nature, both Si wafers and glass are strong possibilities.

Succinctly, a fabrication recipe was elaborated and is described as follows:

A. Cleaning of the substrate [Figure 5.5 (a)]

B. Coating of the substrate with SU-8 photoresist.

C. Spinner for about 40 seconds at varying speeds, depending on the desired thickness [Figure 5.4].

D. Soft bake from 3 to 7 minutes, at 65°C.

E. Natural cooling to room temperature in order to minimize photoresist's failures and undesired textures.

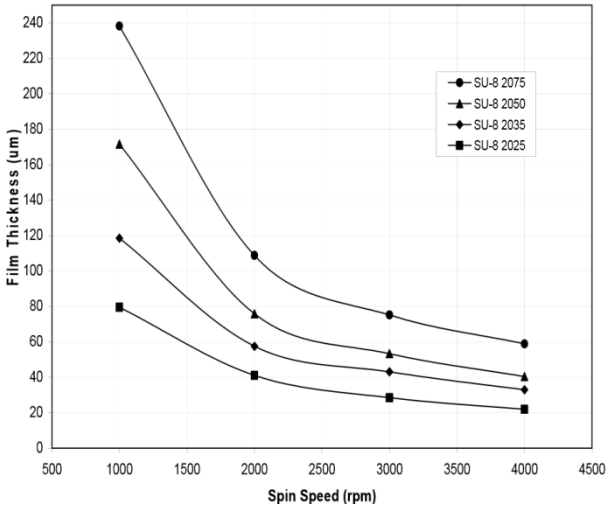

Figure 5.4. SU-8 film thickness as a function of the rotation speed [69].

F. Exposure to the first pattern [Figure 5.5 (b)] either in the direct writing device or a mask aligner.

G. Post exposure bake for 2-5 minutes depending on the thickness.

H. Developing.

I. Deposition of the conductive layer using one of the previously shown techniques.

J. Removal of all the photoresist.

K. Coating of a new layer of photoresist repeating the steps B to E.

L. Exposure to the pattern seen in Figure 5.5 (c) followed by the steps G and H.

This will allow for specific parts of the conductive layer to be exposed, which, in turn, will mean that the p-type pillars will only be deposited in well defined zones. The photoresist layer should be of a thicker nature for this electrodeposition to allow the appearance of lengthily p-type pillars. The

electrolyte used for this process will either be 0% or 40% EG p-type solution, studied in Chapter 3 and will vary depending on the length of the desired pillars and their properties.

M. Without removing the photoresist, a third exposure [Figure 5.5 (d)] is conducted.

The electrodeposition of the n-type pillars is then performed, giving rise to both type of pillars with about the same length. This will also permit for the creation of the characteristic two pillar sequence connected to thermoelectric materials. The electrolyte used for this process will either be 0% or 40% EG n-type solution and will also vary depending on the desired pillar properties and lengths.

N. Forth exposure [Figure 5.5 (e)] followed by the steps G and H.

O. Chemical or physical etching on exposed conductor.

These last two steps are very important to remove the photoresist between the pillars. This is required to assure the zigzag path [Figure 1.2] through the semiconductor Bi_2Te_3 material and to make sure that there is no kind of short-circuit in the device. The kind of etching will depend on the used conductive layer and both should work without the appearance of any major problems due to the reduced thickness of the conductor when compared to either the photoresist or semiconductor material.

P. Coating of new photoresist repeating the steps B to E.

Q. Fifth exposure [Figure 5.5(f)] followed by the steps G and H.

Done in order to fill the gap between the two type of pillars, with a thickness similar to the length of the these structures.

R. Deposition of top conductor.

This will allow for a path for current propagation which involves every pillar in the system.

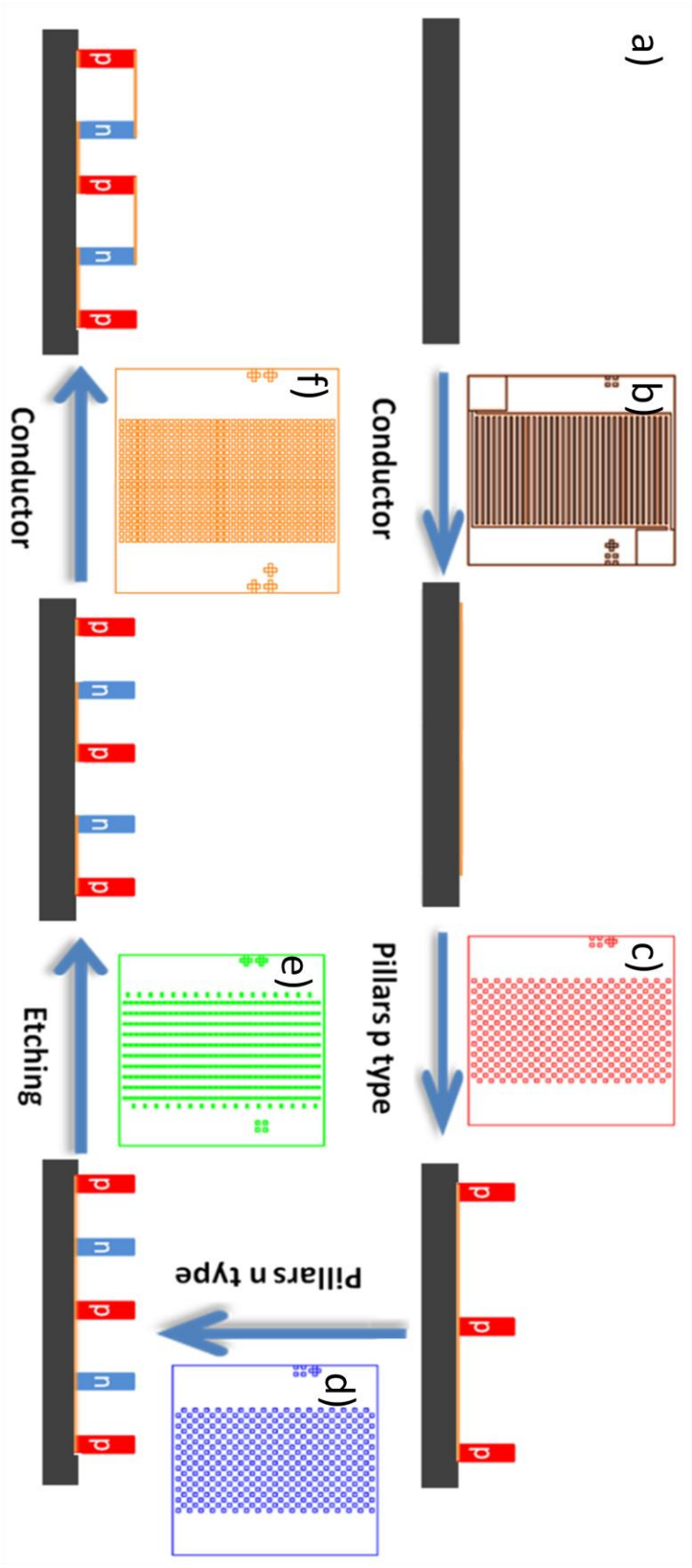

Figure 5.5. Fully functional thermoelectric microgenerator build diagram.

Due to the untested nature of this procedure, small changes and adaptations might need to be done on the procedure explained above. Not only this but further study will then be required to maximize

the generation results of these devices. Variations on pillars height, number of pillars, their area and what conductor is used might strongly influence the resulting outputs. It will possibly be necessary to make a thorough study on the characteristics of the pillars created with each electrolyte to decide the standard one.

5.4 Conclusion

In this chapter it was shown the ability to develop microdevices based on the photolithography and electrodeposition principles showing the first steps towards the main goal. Concerning the first 2 simple prototypes, a study of the generated potentials has been conducted which allow to conclude the existence of p-type and n-type Bi_2Te_3 pillars showing that electrodeposition is an excellent tool to control the stoichiometry of Bi-Te based materials but obtaining a small Seebeck coefficient up to 15 uV/K. Furthermore, from the obtained results we can infer that the bench test set-up of thermoelectric microgenerators is working properly. Finally, with the goal of achieve high performance, flexible and rigid thermoelectric generators, a lithographic recipe was elaborated and explained the methodology that will be addressed of this second device composed by both p and n type semiconductors simultaneously. Nevertheless, we remark that only when the production of the device will be performed, this methology might vary from the explained steps in this work in order to be more fast and efficient always taking into account the industrial scaling.

Chapter 6

Conclusions and future work

6.1 Conclusions

With the major aim of developing the best possible Bi_2Te_3 micro- and nano-structures based on the electrodeposition process, a complete study over nanowires and thin films has been conducted. The thorough research performed on the growth of thin films was successful, with results showing a strong effect of the electrodeposition potential on the samples' properties. Its effect on the morphology and growth pattern was found to be quite significant, resulting in a major cluster-like growth at higher values and a much more homogeneous morphology at lower values. Its influence over thin film thickness and surface roughness is also important, which were found to increase with the applied potential. The XRD results showed a very strong crystalline growth at lower potentials which quickly turned amorphous with the rising of this parameter. The influence of the concentration of the Bi and Te ions on the electrolyte has also been studied. These not only influenced the deposition rate, but also the crystalline growth, sample roughness and typical morphology. The correct stoichiometry for the appearance of both n-type and p-type semiconductors has been achieved, by raising the concentration of Bi in the electrolyte used. An apparatus for the measurement of the Seebeck effect of these structures was then developed and tested in order to better characterize the samples obtained, having been shown that these measurements show a constant measurement error of about 15% on bulk structures. There is still the need to define the best way to measure electrodeposited thin films to guarantee the conductive material below does not affect this measurement.

In the nanowire structures, the optimization of the deposition method and an advanced characterization of the typical growth processes, have been performed. The study of the current transient curves monitored during the NWs deposition allowed a preliminary overall characterization of the samples' quality before the use of expensive techniques such as XRD, SEM and EDS. The deep study of the pore filling as a function of the applied potential was then performed by SEM, as well as its effect on the deposition rate and NWs morphology. The XRD results showed an almost monocrystalline growth at very low potentials, which then turned into an amorphous growth with increasing potentials. For the NWs deposition, only a single electrolyte has been used and the perfect stoichiometry has been reached. The Te% concentration measured by EDS was found to linearly increase with the applied potential, allowing an easy tuning of the final stoichiometry.

Finally, two devices (a p-type and an n-type) have been developed, based on the fabrication of an array of simple pillars using lithographic techniques. The potential output of these samples has also been studied, with the final goal of characterizing and, in the end, developing a fully functional microdevice. As a final point, the design, planning and production methods have been studied and developed aiming future industrialization of the fabrication process.

6.2 Future work

Taking into account the results obtained in this thesis one can now draw some guidelines for future advancements in the thermoelectric materials fabrication and device implementation. In the materials' part, a thorough study of the annealing effects on the resulting samples might prove invaluable for further improvements of the materials structure. In particular, the use of different annealing temperatures might strongly affect the transport properties of the samples. Also, the cooling processes applied can affect the grain size and crystallinity of the sample, thus allowing its optimization. Another possible line of development is the use of different acidic solutions as the electrolyte, which may be less reactive with the conductive materials used as substrates or even the nanoporous alumina template. The downside of this possible line is the fact that the studies done so far on the electrolyte's effects and electrodeposition potential on the resulting samples are expected to vary greatly with the use of a new acid, thus implying new optimization studies. Further work over a conductor or semiconductor capable of creating a high quality thin film/nanowire growth that is able to withstand the solution presented in this work is also a possible line of research.

As for the device's prospects, the possibility to develop a more advanced microgenerator, as shown before, is one the main possible lines of work, which ranges from the complete production method of this device, which is a complex process, to the optimization of its parameters. The optimization of the pillars height, their area, the effective semiconductor area, the conductive layer, photoresist, substrate and many other characteristics, might strongly affect the power output of the device and its costs. Therefore, future work based on the presented results has a lot of possible ways to further develop this principle and to make it a flagship technology.

List of Publications and Communications

Publications

M. Rosmaninho, M.Proença, C.T. Sousa, J. Ventura, J.P.Araújo, L. Fernandes, P.B.Tavares, A.M. Pereira, "Tailoring the Bi-Te Based Nanomaterials by Electrodeposition for Thermoelectric Applications" under preparation.

Oral Communications

"Electrodeposition of Bi2Te3 nanomaterials for thermoelectric generators" Miguel Rosmaninho, Mariana P. Proença, Célia T. Sousa, João Ventura, João P. Araújo, André M. Pereira, 5th International conference on Advanced Nanomaterials (ANM 2014), oral presentation, Aveiro, Portugal, 2-4 July 2014.

"Electrodeposition of Bi2Te3 materials for Thermoelectric micro/nanogenerators" Miguel Rosmaninho, Mariana P. Proença, Célia T. Sousa, João Ventura, João P. Araújo, André M. Pereira, VIII Jornadas IFIMUP-IN, oral presentation, Porto, Portugal, 12 September 2014.

"Electrodeposition of Bi2Te3 Nanomaterials for Thermoelectric generators" M. Rosmaninho, M.P. Proença, C.T. Sousa, J. Ventura, J.P. Araujo, A.M. Pereira, IJUP 2014, oral presentation, Porto, Portugal, 12 February 2014.

Poster communications

"Electrodeposition of Bi2Te3 Nanomaterials for Thermoelectric Generators" M. Rosmaninho, M.P. Proença, C.T. Sousa, J. Ventura, J.P. Araújo and A.M. Pereira, International Workshops in Electrodeposited Nanostructures (EDNANO 2014), poster presentation, Oberwesel am Rhein, Germany, 20-22 March 2014.

Other scientific work

Finalist of the competition for innovative ideas in the Univerisity of Porto (iUP25k) with the project inanoE.

http://iup25k.up.pt/2014/

Finalist in the IDEup competition for most innovative projects in universities Ibero-American hosted by the REDEMPREDIA Spin 2014 with the project inanoE.

http://www.redemprendia.org/pt/spin/spin2014/ideup

Recipient of the "Passaporte para o Empreendorismo" grant due to the inanoE project.

http://www.passaporteempreendedorismo.pt/index/

Co-founder of the inanoE project, a spin-off localized at University of Porto, where we achieve to design, develop and produce micro generators based on the piezo, thermo or triboelectric effect designed and created for each client.

References

1 ObservatoryNANO Briefing.(2011). Observatory NANO Briefing, June 2011 (17), 1–4.

2 *bp statistical review of World Energy (2012).*

3 Venkatasubramanian, R., Silvola, E., Colpitts, T. & O'Quinn. (2001). Thin-Film thermoelectric devices with high room-temperature figure of merit. Nature 413, 597–602.

4 Martín-González, M., Caballero-Calero, O., & Díaz-Chao, P. (2013). Nanoengineering thermoelectrics for 21st century: Energy harvesting and other trends in the field. Renewable and Sustainable Energy Reviews, 24, 288–305.

5 Harman, T.C.. (2002). Quantum dot superlattice thermoelectric materials and devices. Science 297, 2229.

6 Boukai, A.I.. (2008). Silicon nanowires as efficient thermoelectric materials Nature, 451, 168.

7 Eder, A. (2009). Thermoelectric Power Generation - The Next Step to Future CO 2 Reductions ?! BMW Efficient Dynamics.

8 Corporation, F. H. (2013). Sustainability Report 2013.

9 Yang, J., Yip, H.-L., & Jen, A. K.-Y. (2013). Rational Design of Advanced Thermoelectric Materials. Advanced Energy Materials, 3(5), 549–565.

10 Tritt, T. M. (2011). Thermoelectric Phenomena, Materials, and Applications. Annual Review of Materials Research, 41(1), 433–448.

11 Kanatzidis, M.G. (2010). Nanostructured thermoelectrics: The new paradigm? Chemistry of Materials, 22(3), pp. 648-659.

12 Kraemer, D., Poudel, B., Feng, H., Caylor, J. C., Yu, B., Yan, X.,Chen, G. (2011). generators with high thermal concentration, 10(July).

13 Goldsmid, H. J. (1964). Thermoelectric Refrigeration (Plenum).

14 Heremans, J.P., Dresselhaus, M.S., Bell, L.E. and Morelli, D.T. (2013). When thermoelectrics reached the nanoscale. Nature Nanotechnology, 8(7), pp. 471-473.

15 Chen, Z.G., Han, G., Yang, L., Cheng, L., & Zou, J. (2012). Nanostructured thermoelectric materials: Current research and future challenge. Progress in Natural Science: Materials International, 22(6), 535–549.

16 https://webberenergyblog.wordpress.com/author/hfateh/, visited 23-09-14

17 Zheng, J. (2008). Recent advances on thermoelectric materials. Frontiers of Physics in China, 3(3), 269–279.

18 Alam, H., & Ramakrishna, S. (2013). A review on the enhancement of figure of merit from bulk to nano-thermoelectric materials. Nano Energy, 2(2), 190–212.

19 Feldman, J. L., Singh, D. J., Mazin, II, Mandrus, D. & Sales, B. C. (2000). Lattice dynamics and reduced thermal conductivity of filled skutterudites. Phys. Rev.B 61, R9209‑R9212.

20 Terasaki I, IwakawaM, Nakano T, Tsukuda A, KobayashiW. (2010). Novel thermoelectric properties of complex transition-metal oxides. Dalton Trans. 39(4):1005–11.

21 Xie, W., Tang, X. , Yan, Y., Zhang, Q., Tritt, T.M.. 94 (2009) . Unique nanostructures and enhanced thermoelectric performance of melt-spun BiSbTe alloys, Applied Physics Letters 102111.

22 Shakouri, A. (2011). Recent Developments in Semiconductor Thermoelectric Physics and Materials. Annual Review of Materials Research, 41(1), 399–431.

23 Hsu , K. F., Loo, S., Guo, F., Chen, W., Dyck, J. S., Uher, C., Hogan, T., Polychroniadis, E. K., Kanatzidis, M. G. (2004). "Cubic AgPbmSbTe2+m: bulk thermoelectric materials with high figure of merit". Science, 303 818

24 W. Xie, X. Tang, Y. Yan, Q. Zhang, T.M. Tritt (2009), Unique nanostructures and enhanced thermoelectric performance of melt-spun BiSbTe alloys, Applied Physics Letters 94 102111.

25 Chen, Z.-G., Han, G., Yang, L., Cheng, L., & Zou, J. (2012). Nanostructured thermoelectric materials: Current research and future challenge. Progress in Natural Science: Materials International, *22*(6), 535–549. doi:10.1016/j.pnsc.2012.11.011

26 Hicks, L.D., Harman, T.C., Sun, X., Dresselhaus, M.S. (1996). Experimental study of the effect of quantum-well structures on the thermoelectric figure of merit. Physical Review B 53 (16).

27 Mingo, N. (2004). Thermoelectric figure of merit and maximum power factor in III-V semiconductor nanowires. Applied Physics Letters. 84, 2652.

28 Hicks, L.D. & Dresselhaus, M.S. (1993). Effect of quantum-well structures on the thermoelectric figure of merit. Physical Review B, vol. 47, no. 19, pp. 12727-12731.

29 Sparks, T. (2008). Thermoelectric supperlattices. Materials 265, Nov 19 2008.

30 Boukai, A. I., Bunimovich, Y., Tahir-Kheli, J., Yu, J.-K., Goddard, W. a, Heath, J. R. (2008). Silicon nanowires as efficient thermoelectric materials. Nature, 451(7175), 168–71.

31 Kim, S.J., We, J.H. & Cho, B.J. 2014, "A wearable thermoelectric generator fabricated on a glass fabric", Energy and Environmental Science*,* vol. 7, no. 6, pp. 1959-1965.

32 Kim, M.K., Kim, M.S., Jo, S.E., Kim, H.L., Lee, S.M. & Kim, Y.J. 2013, "Wearable thermoelectric generator for human clothing applications", 2013 Transducers and Eurosensors XXVII: The 17th International Conference on Solid-State Sensors, Actuators and Microsystems, TRANSDUCERS and EUROSENSORS *2013*, pp. 1376.

33 Corey A. Hewitt, Alan B. Kaiser, Siegmar Roth, Matt Craps, Richard Czerw, and David L. Carroll 2012, "Multilayered Carbon Nanotube/Polymer Composite Based Thermoelectric Fabrics", Nano Letters, 2012, 12 (3), pp 1307–1310.

34 Peranio, N., Leister, E., Töllner, W., Eibl, O., Nielsch, K., (2012). Stoichiometry controlled, single-crystalline Bi 2Te 3 nanowires for transport in the basal plane. Advanced Functional Materials, 22(1), pp. 151-156.

35 Siegal, M.P., Limmer, S.J., Lensch-Falk, J.L., Erickson, K.J., Medlin, D.L., Yelton, W.G., Rochford, C., (2014). Improving Bi2Te3-based thermoelectric nanowire microstructure via thermal processing. Journal of Materials Research, , pp. 1-8.

36 Wang, Z., Ruhhammer, J., Adhikari, S., Rostek, R., Moser, D., Paul, O., Kojda, D., Mitdank, R., Fischer, S.F., Toellner, W., Nielsch, K., Kroener, M. & Woias, P. 2013, "Thermoelectric Properties Investigation of Single nanowires by utilizing a Thermoelectric Nanowire Characterization Platform", 8th Annual IEEE International Conference on Nano/Micro Engineered and Molecular Systems, IEEE NEMS 2013, pp. 738.

37 Fang, H., Feng, T., Yang, H., Ruan, X. & Wu, Y. 2013, "Synthesis and thermoelectric properties of compositional-modulated lead telluride-bismuth telluride nanowire heterostructures", *Nano Letters,* vol. 13, no. 5, pp. 2058-2063.

38 Hsin, C.-., Wingert, M., Huang, C.-., Guo, H., Shih, T.-., Suh, J., Wang, K., Wu, J., Wu, W.-. & Chen, R. 2013, "Phase transformation and thermoelectric properties of bismuth-telluride nanowires", *Nanoscale,* vol. 5, no. 11, pp. 4669-4672.

39 Chen, C., Chen, Y., Lin, S., Ho, J.C., Lee, P., Harutyunyan, S.R., (2010). Fabrication and characterization of electrodeposited bismuth telluride films and nanowires. Journal of Physical Chemistry C, 114(8), pp. 3385-3389.

40 Li, S., Toprak, M.S., Soliman, H.M.A., Zhou, J., Muhammed, M., Platzek, D., Müller, E., (2006). Fabrication of nanostructured thermoelectric bismuth telluride thick films by electrochemical deposition. Chemistry of Materials, 18(16), pp. 3627-3633.

41 Tittes, K., Bund, A., Plieth, W., Bentien, A., Paschen, S., Plötner, M., Gräfe, H. and Fischer, W., (2003). Electrochemical deposition of Bi2Te3 for thermoelectric microdevices. Journal of Solid State Electrochemistry, 7(10), pp. 714-723.

42 Peranio, N., Leister, E., Töllner, W., Eibl, O. & Nielsch, K. 2012, "Stoichiometry controlled, single-crystalline Bi 2Te 3 nanowires for transport in the basal plane", Advanced Functional Materials, vol. 22, no. 1, pp. 151-156

43 Takahashi, M., Kojima, M., Sato, S., Ohnisi, N., Nishiwaki, A., Wakita, K., Miyuki, T., Ikeda, S. & Muramatsu, Y. 2004, "Electric and thermoelectric properties of electrodeposited bismuth telluride (Bi2Te3) films", Journal of Applied Physics, vol. 96, no. 10, pp. 5582-5587.

44 Bard, A. J., Faulkner, L. R. (2001). Electrochemical Methods Fundamentals and Applications.

45 Mariana P. Proença 2012, "Magnetism at the Nanoscale: Nanoparticles, Nanowires, Nanotubes and their Ordered Arrays", Phd thesis.

46 A. Holleman, N. Wiberg, "Inorganic Chemistry", Academic Press, 2001

47 Li, S., Toprak, M.S., Soliman, H.M.A., Zhou, J., Muhammed, M., Platzek, D. & Müller, E. 2006, "Fabrication of nanostructured thermoelectric bismuth telluride thick films by electrochemical deposition", Chemistry of Materials, vol. 18, no. 16, pp. 3627-3633.

48 Leitao, D.C., Sousa, C.T., Ventura, J., Carpinteiro, F., Correia, J.G., Amado, M.M., Sousa, J.B. & Araujo, J.P. 2008, "Influence of surface pre-treatment in the room temperature fabrication of nanoporous alumina", Physica Status Solidi (C) Current Topics in Solid State Physics, vol. 5, no. 11, pp. 3488-3491.

49 Leitao, D.C., Apolinario, A., Sousa, C.T., Ventura, J., Sousa, J.B., Vazquez, M. & Araujo, J.P. 2011, "Nanoscale topography: A tool to enhance pore order and pore size distribution in anodic aluminum oxide", Journal of Physical Chemistry C, vol. 115, no. 17, pp. 8567-8572.

50 Leitao, D.C., Ventura, J., Sousa, C.T., Teixeira, J.M., Sousa, J.B., Jaafar, M., Asenjo, A., Vazquez, M., De Teresa, J.M. & Araujo, J.P. 2012, "Tailoring the physical properties of thin nanohole arrays grown on flat anodic aluminum oxide templates", Nanotechnology, vol. 23, no. 42.

51 Sousa, C.T., Leitão, D.C., Proença, M.P., Apolinário, A., Correia, J.G., Ventura, J. & Araújo, J.P. 2011, "Tunning pore filling of anodic alumina templates by accurate control of the bottom barrier layer thickness", Nanotechnology, vol. 22, no. 31.

52 Proenca, M.P., Sousa, C.T., Ventura, J., Vazquez, M. & Araujo, J.P. 2012, "Ni growth inside ordered arrays of alumina nanopores: Enhancing the deposition rate", Electrochimica Acta, vol. 72, pp. 215-221.

53 H. Masuda and K. Fukuda 1995, “Ordered metal nanohole arrays made by a two-step replication of honeycomb structures of anodic alumina”, Science, vol. 268, pp. 1466–1468.

54 Jean M. Bennett, Lars Mattsson, Introduction to Surface Roughness and Scattering, Optical Society of America, Washington, D.C.

55 Joseph Goldstein 2003, Scanning Electron Microscopy and X-Ray Microanalysis. Springer. ISBN 978-0-306-47292-3.

56 B.D. Cullity & S.R. Stock 2001, "Elements of X-Ray Diffraction", 3rd Ed., Prentice-Hall Inc., , p 167-171

57 Rodriguez-Carvajal 1993, Journal Physica B., 192, 55

58 Jaeger, Richard C 2002, "Film Deposition". Introduction to Microelectronic Fabrication (2nd ed.).

59 Harsha, K.S.S. 2006, "Principles of Physical Vapor Deposition of Thin Films", Elsevier, Great Britain, p.400

60 Safa Kasap , 1997 "Thermoelectric Effects in Metals: Thermocouples",e-Booklet

61 Moffat, R. 1997, “Notes on Using Thermocouples”, ElectronicsCooling, Vol. 3, No. 1

62 Martín-González, M.S., Prieto, A.L., Gronsky, R., Sands, T. & Stacy, A.M. 2002, "Insights into the electrodeposition of Bi2Te3", Journal of the Electrochemical Society, vol. 149, no. 11, pp. C546-C554.

63 Dinnebier, R. 2008, "Powder Diffraction: Theory and Practice" (1st ed.)

64 Rowe, D. M. 1995, "CRC Handbook of Thermoelectrics", CRC Press, Boca Raton, FL, , ch. 19.

65 H. P. Nguyen, J. Su, Z. Wang, R. J. Vullers, P. M. Vereecken, and J. Fransaer, Journal of Materials Research, 26(15), 1953 (2011).

66 Miyazaki, Y. & Kajitani, T. 2001, "Preparation of Bi2Te3 films by electrodeposition", *Journal of Crystal Growth,* vol. 229, no. 1, pp. 542-546.

67 Yoo, B.Y., Huang, C.-, Lim, J.R., Herman, J., Ryan, M.A., Fleurial, J.-. & Myung, N.V. 2005, "Electrochemically deposited thermoelectric n-type Bi2Te 3 thin films", Electrochimica Acta, vol. 50, no. 22, pp. 4371-4377.

68 Sulka, G.D. and Parko, K.G. (2007) Electrochim. Acta,52, 1880–1888.

69 SU-8 2000 Permanent Epoxy Negative Photoresist datasheet